Earth-Science Reviews 254 (2024) 104815

Contents lists available at ScienceDirect

Earth-Science Reviews

journal homepage: www.elsevier.com/locate/earscirev

Post glacial sediment partitioning on a tectonically controlled, narrow shelf (Calabro-Tyrrhenian margin, Italy): Issues in defining S2S budget

Daniele Casalbore [a,b], Eleonora Martorelli [b,*], Domenico Ridente [b], Romano Clementucci [c], Francesco Latino Chiocci [a,b]

[a] Dipartimento di Scienze della Terra, Sapienza Università di Roma, Rome, Italy
[b] CNR-IGAG, Sede Università Sapienza di Roma, Rome, Italy
[c] ETH Zurich, Department of Earth Sciences, Zurich, Switzerland

ARTICLE INFO

Keywords:
Seismic stratigraphy
Source-to-sink
Sediment budget
Continental shelf
Last glacial maximum
Calabria

ABSTRACT

The re-analysis of high-resolution seismic profiles collected along the narrow (2–9 km) shelf facing ~90 km of the Calabro-Tyrrhenian coastline has enabled the reconstruction of its sequence-stratigraphic architecture, along with the quantification of sediment volumes accommodated during the last post-glacial sea level rise and highstand. The shelf volumes are compared with the gross volumes supplied by the short and steep rivers draining the uplifted hinterland area, obtained from morphometric analysis and inferred denudation rates (derived from uplift rates) of the drainage basins. The study area is divided in two main sectors based on the different morpho-stratigraphic setting and fluvial network controlling sediment distribution on the shelf. The Coastal Range sector is characterized by closely spaced mountainous rivers and narrow coastal plains; on the shelf, the post-LGM deposits show a main depocenter (up to 60 m thick) elongated ~27 km parallel to the coastline. This shelf sector hosts up to 80% of the sediment sourced from rivers, with a small percentage of sediment loss, mainly related to off-shelf export along a network of shelf-indenting submarine canyons. Sediment deficit due to river aggradation is considered negligible based on the narrow and V-shaped thalwegs typical of the rivers in this sector. The Santa Eufemia sector is characterized by larger rivers and a wider coastal plain, with a major depocenter (up to 50 m thick) confined off the Amato River. In this sector, the entire post-LGM sequence accounts only for about 30% of the sediment supplied by rivers (60% considering only the HST), indicating that, in addition to sediment exported off-shelf, a significant part is trapped by river aggradation within the coastal plain. The volumetric comparison has also evidenced local but significant discrepancies in sedimentary budget between adjacent sub-sectors, likely related to the effect of northward-directed shelf currents on sediment distribution along the shelf.

1. Introduction

In geology, the source-to-sink (hereafter S2S) concept was first introduced by Meade (1972) to quantify the sediment supply to the coastline and shelf of the eastern USA margin during the late Holocene. Since then, many S2S studies were carried out in siliciclastic systems (e.g., Walsh et al., 2016 and reference therein) and, to a minor extent, also in carbonate reefs (e.g., Perry et al., 2015 and reference therein) and insular volcanic settings (e.g., Manville et al., 2009; Romagnoli et al., 2012). The main purpose of S2S studies is to provide an integrated perspective of erosional-depositional systems, encompassing the connections between the different segments from the source area to the final depositional sink (e.g., Allen, 2008; Somme et al., 2009). In marine settings, a key role for S2S studies has been played by sequence stratigraphy analysis as developed by the Exxon group (e.g., Vail et al., 1984; Van Wagoner et al., 1988; Van Wagoner et al., 1990) and later redefined or critically reviewed (e.g., Hunt and Tucker, 1992; Helland-Hansen and Martinsen, 1996; Lobo and Ridente, 2014; more details in the Appendix). Sequence stratigraphy models allow the breakdown of sedimentary bodies into genetic units separated by key stratigraphic surfaces reflecting specific mechanisms ultimately (though not exclusively) related to base level change and its interplay with supply (e.g., Catuneanu et al., 2009). These units and key stratigraphic surfaces provide means for modelling of temporal and spatial variations in

* Corresponding author.
E-mail address: eleonora.martorelli@cnr.it (E. Martorelli).

https://doi.org/10.1016/j.earscirev.2024.104815
Received 1 August 2023; Received in revised form 2 May 2024; Accepted 10 May 2024
Available online 18 May 2024

sediment supply across a basin (e.g., Gamberi and Marani, 2006; Ballato and Strecker, 2014).

The S2S studies integrate these changes in sedimentation across a basin within a quantitative assessment of sedimentary budgets throughout all the segments composing the S2S route, each mutually dependent although deemed as distinct sections (e.g., Sømme et al., 2011; Blum and Womack, 2009). This analysis is generally accomplished by integrating the geomorphic analysis of terrestrial and marine basins with seismic-stratigraphic and sedimentary analysis to define sediment routing, partitioning, and storage along the entire S2S system for a given time interval (e.g., Helland-Hansen et al., 2016). S2S studies have been applied at a wide range of spatial (from single river catchment to orogenic regional scale) and time scales (from 10^1 to 10^6 of years), depending on the objectives, available data, and methodological constraints.

In this study, we attempt a S2S approach based on the application of high-resolution sequence-stratigraphic analysis for estimating the sedimentary budget across a narrow shelf sector extending 90 km along the tectonically controlled Calabro-Tyrrhenian margin (Fig. 1) during the last eustatic hemicycle, i.e. since the Last Glacial Maximum (LGM,

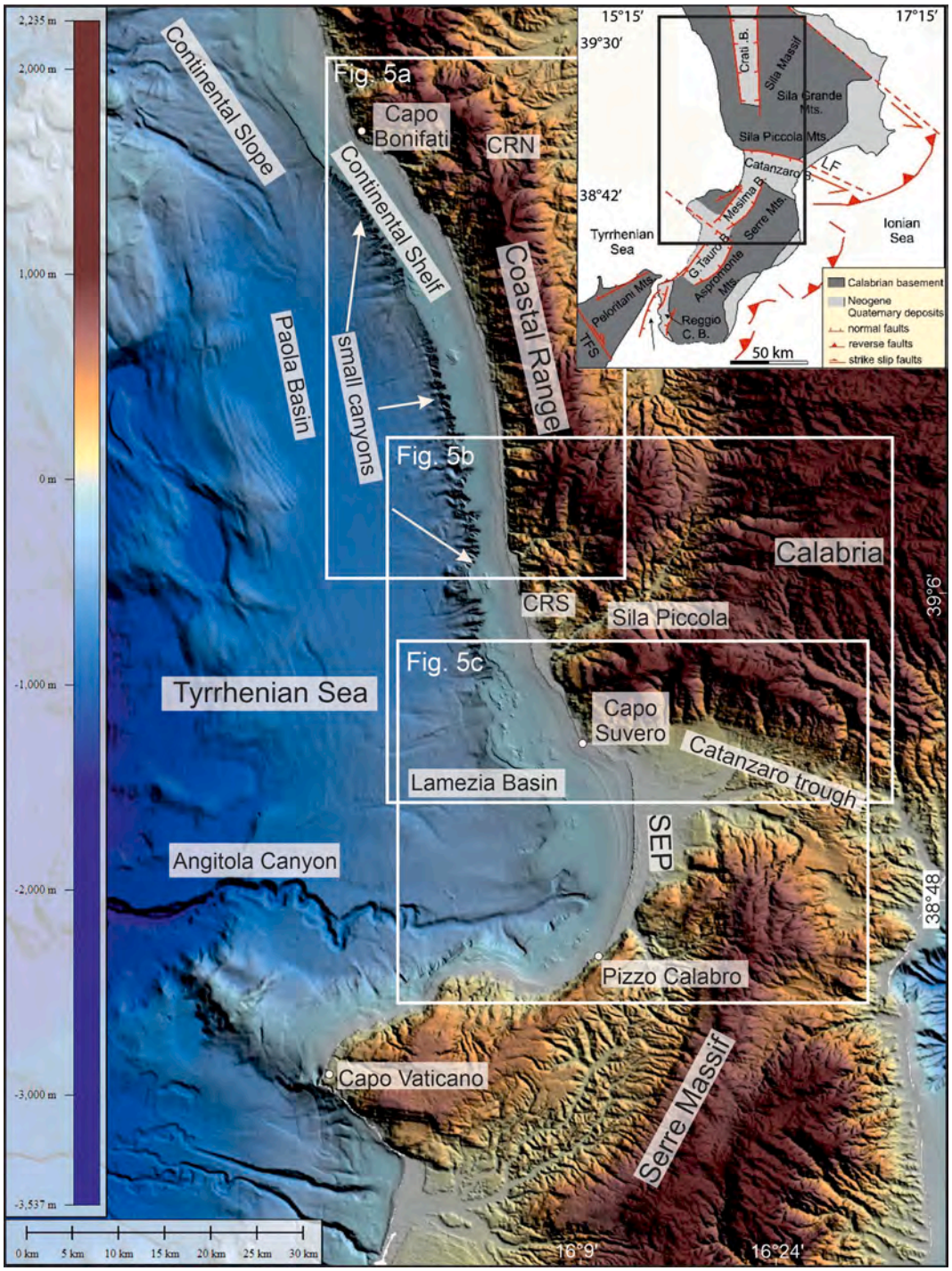

Fig. 1. Shaded relief map (artificial light from NE) of the study area, obtained by merging ASTER G-DEM topographic data with multibeam data from EMODNET Bathymetry and MaGIC project, with the indication of the main morphological features and locations of the following figures. In the inset, a simplified map displaying the main structural elements of the Calabrian arc after Pirrotta et al. (2022). TFS: Tindari Fault System LF: Lamezia Fault.

hereafter). The shelf sediment volumes derived from the re-analysis of a large dataset of high-resolution seismic profiles (Fig. 2) integrated with those estimated on the coastal plains are compared with the gross sediment volumes sourced from the fluvial system. This volumetric comparison allows us to constrain the main factors responsible for sediment delivery and dispersal across and along this shelf during the sea level rise and highstand. Quantifying sediment delivery, storage, and export from continental shelves has also implications both on the preservation of river-sourced organic carbon on the shelf (Kuehl et al., 2016) and deep-water sedimentation (e.g., Nittrouer, 2003).

2. Geological setting

The study area is located along the Tyrrhenian side of the Calabrian Arc (Fig. 1), which is an allochthonous crustal block overriding the Southern Apennine domain during the Neogene subduction and roll-back of the west-dipping Ionian slab (e.g., Doglioni et al., 1996; Faccenna et al., 2011). The Calabrian arc recorded regional uplift since the Pleistocene (e.g., Westaway, 1993; Antonioli et al., 2006) and is characterized by frequent and strong seismicity (DISS Working Group, 2021). Because of this uplift, a network of steep and short rivers (locally named Fiumara, Sabato and Tropeano, 2004) is formed; they are characterized by a seasonal torrential regime. Within the above tectonic frame, the study area extends across two main sectors: one to the north dominated by the Coastal Range (CR, hereafter) and one to the south where the large Santa Eufemia Plain (SEP, hereafter) is present.

2.1. Coastal range

The CR is a narrow mountain belt that extends for about 700 km^2 along a N-S direction (Fig. 1). It mainly consists of ophiolitic and metamorphic units piled up and unconformably overlapped by Tertiary to Quaternary sedimentary deposits (e.g., LePera and Critelli, 1997). The landscape of the CR is characterized by fault scarps, structural cliffs, steep and V-shaped river catchments, and alluvial fans prograding onto a very narrow coastal plain (e.g., Sorriso-Valvo and Sylvester, 1993; Muto et al., 2003). Active alluvial fans are mostly concentrated along the coast, while older generations of dissected fans are recognizable along the piedmont area (Robustelli et al., 2005). During the last few thousands of years, the geomorphological evolution of the area has been also controlled by anthropic activity (e.g., Sorriso-Valvo and Sylvester, 1993). Based on the morphological features, the CR can be further divided into northern (CRN) and southern (CRS) sub-sectors (Fig. 1). The CRN is characterized by a tight network of short rivers and very narrow coastal plains, while the CRS shows longer rivers and larger coastal plains.

2.2. The Santa Eufemia Plain

The SEP is elongated for ~20 km (Fig. 1) and, together with the offshore area, has been interpreted as a graben-like system, formed during a Middle-Upper Pleistocene extensional tectonic phase within the Catanzaro Trough (Lamezia Basin in Fig. 1; Brutto et al., 2016). A flight of marine terraces is recognizable all along the coast and in the inner sector of the SEP (e.g., Meschis et al., 2022 and reference therein). The piedmont zone of the SEP mainly consists of Late Pleistocene-Holocene alluvial fans; the coastal area shows low slope gradients and is dominated by alluvial sedimentation linked to the Amato River.

The Holocene history of the SEP has been reconstructed and related to the interaction between eustasy and tectonics (Ruello et al., 2017). Specifically, a marked environmental transition at 6900 yr. cal BP was observed: a first stage characterized by coastline ingression and aggradation, due to eustasy largely overwhelming tectonic uplift, is followed by a second stage (between 6900 and 2800 yr. cal BP) dominated by coastline progradation and aggradation due to a combination of high detrital inputs, slowdown of sea level rise, and subsidence rates. Later

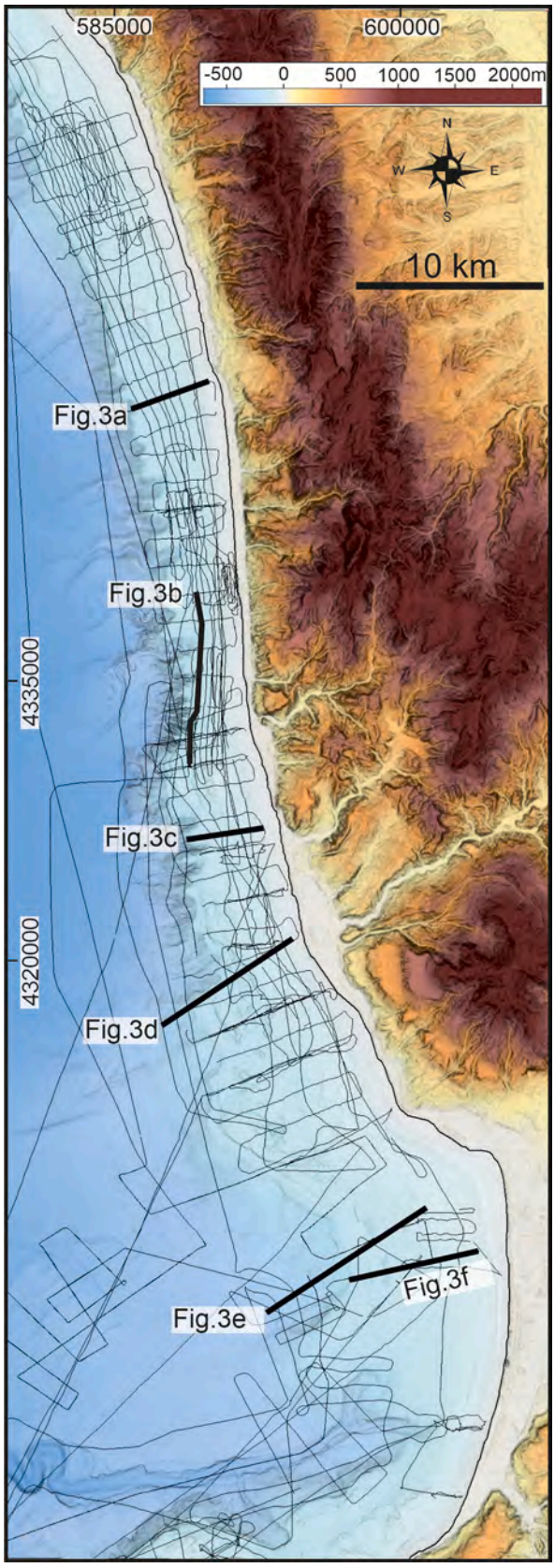

Fig. 2. Database of seismic profiles at different resolution and penetration available for this study; the bold lines indicate the trace of the seismic profiles shown in Fig. 3.

the SEP was characterized by overall stability, punctuated by local variations due to the interaction between short-term climatic changes, local tectonic processes and anthropic activity (Ruello et al., 2017).

2.3. The continental shelf

The continental margin is characterized by a 2–9 km wide continental shelf, overall composed by siliciclastic prograding units (Fig. 3) mainly recording Plio-Pleistocene lowstand and forced regressive phases (Chiocci et al., 1989). The post-LGM deposits form a wedge-shaped depositional unit, bounded at its base by a high-amplitude and high continuity reflector that unconformably truncates the underlying Plio-Pleistocene prograding units (Chiocci et al., 1989; Martorelli et al., 2010). This reflector has regional extent and was interpreted as the LGM unconformity (LGM-U in Fig. 3) formed during subaerial erosion and subsequent transgressive reworking. The post-LGM unit include deposits of the transgressive systems tract (TST) and high-stand systems tract (HST). It covers almost entirely the continental shelf, thinning towards the shelf break; this appears draped by relatively thin deposits (e.g., a few meters thick) over most of the study area (Fig. 3).

The TST consists of 2–3 backstepping parasequences separated by flooding or erosional (ravinement) surfaces, generally characterized by high-continuity, high-amplitude reflectors and downlap terminations (Fig. 3a and c). The upper boundary is marked by the Maximum Flooding Surface (MFS in Fig. 3), which is a downlap surface with a sigmoidal to concave-up dip profile. Typically, the TST parasequences are laterally confined by the irregularities of the LGM-U (Fig. 3d and f), which often arrive at or close to the seafloor. These irregularities can be used as substrate for the subsequent development of build-up structures, as suggested by dredged materials recovered at their summit (Martorelli et al., 2010).

The HST is composed of two prograding parasequences. The lower parasequence is generally characterized by low-amplitude reflectors or semi-transparent seismic facies (Fig. 3a and c). The upper parasequence is characterized by high continuity-high amplitude reflectors, although spots of transparent seismic facies are also observed. Off river mouths, the occurrence of discontinuous or wavy internal reflectors with very high amplitude may likely reflect coarser sediment; acoustic blanking is also observed, indicating gas-charged sediment (Fig. 3d).

Below the shelf edge, the continental slope is steep (up to 12°) and carved by a network of narrow shelf indenting canyons, debouching into the Paola Basin at about 700 m water depth (Casalbore, 2024). A thin drape (average thickness of 2 m) of Holocene deposits is recognizable both on the slope and basinal areas (Trincardi et al., 1995).

2.4. Oceanographic setting

The study area is characterized by a microtidal regime (tidal range < 20 cm); wave climate reconstructed over the last 40 years indicates that the study area is dominated by westerly winds able to generate

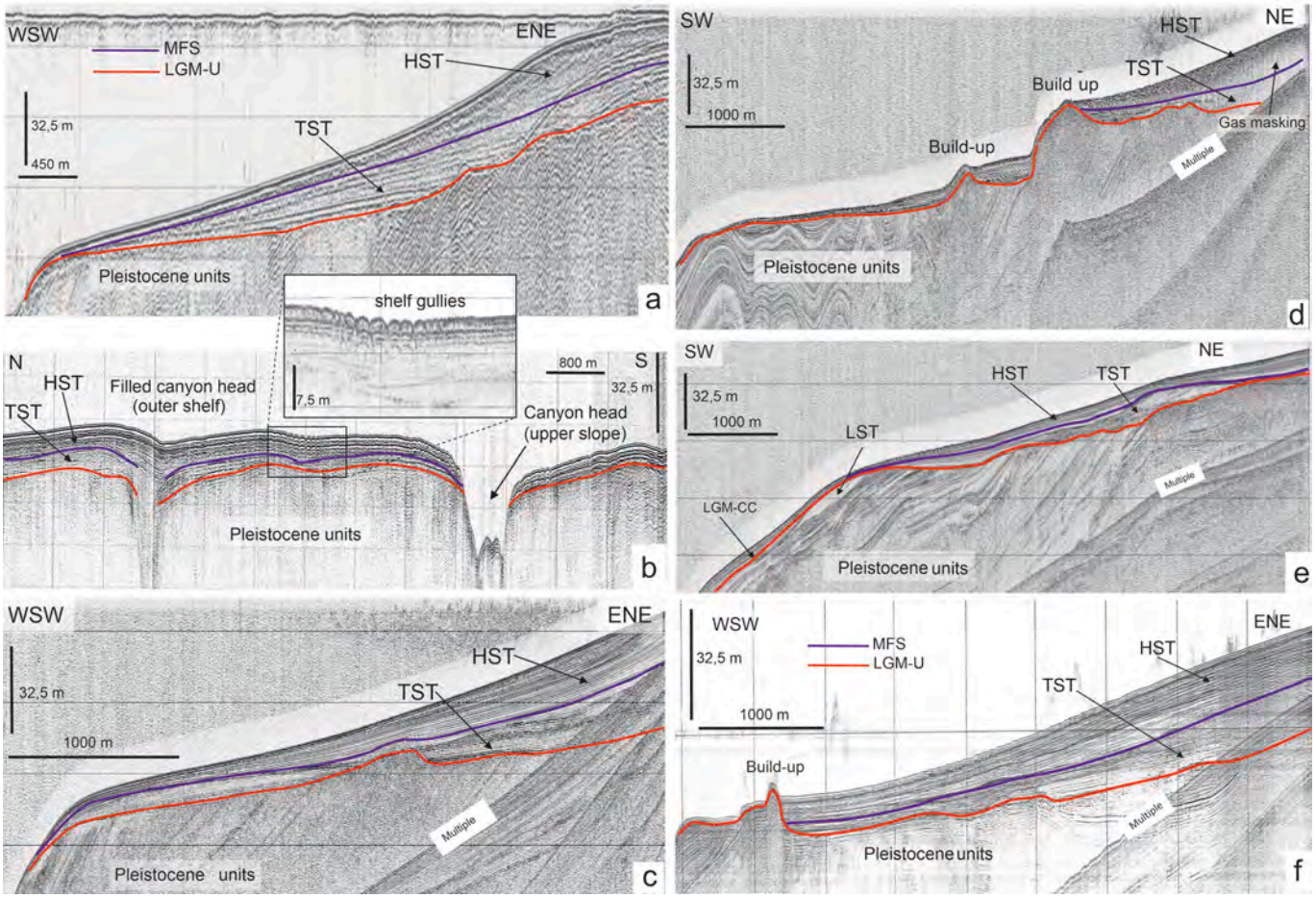

Fig. 3. Sparker seismic profiles carried out perpendicular **(a)** and parallel **(b)** to the shelf in the CRN (location in Fig. 2), with indication of the main reflectors and seismic units used for volumetric computation. Note in strike profile 3b the presence of active and inactive (filled) canyon heads as well as the occurrence of gullies (shown also in higher resolution CHIRP profiles) in the outer shelf. **c)** and **d)** Sparker seismic profiles carried out perpendicular to the shelf in the CRS, with indication of the main reflectors and seismic units used for volumetric computation. **e)** and **f)** Sparker seismic profiles performed perpendicular to the shelf in the SEP, with indication of the main reflectors and seismic units used for volumetric computation. Note the different geometry and higher thickness of the TST and HST units off the Amato River mouth in 3 f.

maximum significant wave heights of 8–9 m and peak periods around 5.6 s during extreme events (Foti et al., 2022). Stormy conditions generally occur during winter, generating mainly wave fields traveling from WSW-WNW directions. The highest waves (offshore height > 5 m) propagate from WSW due to higher fetch distance (1300 km) and their height is amplified nearshore because of shoaling effects (Ietto et al., 2018). Satellite images (Copernicus: Sentinel-2; https://www.copernicus.eu/en/copernicus-satellite-data-access) show a frequent deflection towards the north of river plumes during high river runoff. LePera and Critelli (1997) indicate that the littoral drift is mainly oriented towards the south off the Coastal Range and towards the north in the S. Eufemia Gulf.

The main oceanographic currents consist of two geostrophic flows along the Calabro-Tyrrhenian shelf and upper part of the continental slope: the Atlantic Water (AW) and the Levantine Intermediate Water (LIW). The AW is a 100–200 m surface layer entering the Mediterranean Sea from the Gibraltar Strait and flowing in the Tyrrhenian Sea with a seasonal and annual variability (e.g., Pinardi et al., 1997). During the winter it flows towards the north, during the summer the flow weakens and an anticyclonic pattern develops (Pinardi and Masetti, 2000). The LIW is generated in the Levantine Basin during winter and flows cyclonically sub-parallel to the Calabro-Tyrrhenian margin at a depth range of 200–700 m (e.g., Millot, 1991).

3. Data and methods

3.1. River metrics and catchment analysis

To quantify the terrestrial supply systems (shape of drainage basins and hydrology), a morphometric analysis of the drainage catchments was performed. We used the ASTER GDEM (https://asterweb.jpl.nasa.gov/gdem.asp), ~30 m in resolution, to define the regional topography and extract the drainage network. Averaged-basin analysis was conducted with ArcGIS and MATLAB scripts TopoToolbox (Schwanghart and Scherler, 2014; Forte and Whipple, 2019). We also extracted longitudinal profiles of the rivers to describe their shape and steepness, and gain information about the fluvial response to regional uplift and bedrock erodibility (Duvall et al., 2004; Wobus et al., 2006; Kirby and Whipple, 2012; Clementucci et al., 2022b). At steady-state (or quasi steady-state), the erosion rates are in balance with the rock-uplift rate; according to the stream power model, relationship between the river slope and its drainage area is (Flint, 1974):

$$S = k_s A^{-\theta} \quad (1)$$

where S is the channel slope, A is the contributing drainage area, and k_s and θ are the steepness and concavity indexes. Also, $\theta = m/n$ and $ks = (U/K)^{1/n}$; where m and n are constants depending on basin hydrology, channel geometry and erosion processes (Whipple and Tucker, 1999); U and K are the rate of uplift and erodibility coefficient, respectively; the latter depending on bedrock lithology, climate and sediment load. The relationship in Eq. (1) is valid above a critical upstream drainage area of 0.1–5 km^2, where fluvial processes dominate over debris flow processes (Montgomery and Foufoula-Georgiou, 1993; Stock and Dietrich, 2003). In our case, we used a critical drainage area of 1 km^2.

Because small variations in the concavity index led to large variations in ks, we used a reference concavity index (θ_{ref}) of 0.45 (Wobus et al., 2006; Kirby and Whipple, 2012) to estimate the normalized channel steepness values (k_{sn}; Cyr et al., 2014; Olivetti et al., 2012). In areas with similar climate and lithologic types, k_{sn} mainly reflects the values of uplift rates (e.g., Kirby and Whipple, 2012; Clementucci et al., 2023). Annual mean precipitation rates were extracted from WorldClim database (Hijmans et al., 2005; http://www.worldclim.org/bioclim) using the 30 arc-second (~1 km) resolution grid. All the morphometric parameters are reported in Table S1.

3.2. Marine dataset

The marine dataset consists of bathymetric data and a dense network of high-resolution single-channel seismic reflection profiles (Fig. 2).

Bathymetric data were collected in the ~40–500 m depth range between 2010 and 2012 onboard R.V. Minerva1 and Maria Grazia (CNR). Data were DGPS-positioned, processed, and gridded to obtain DEMs with cell-size variable from 1 m in shallow water depths (between ~40 and 100 m) to 10 m in intermediate water depths (100–500 m). Multibeam data in the nearshore area were merged with bathymetric data obtained from nautical charts, by this generating a final DEM of the shelf and upper slope with a cell-size of 50 m, comparable in resolution with the subaerial ASTER G-DEM.

High-resolution, single-channel seismic profiles (variably spaced from 500 to 2000 m) were collected from ~40 m water depth down to the shelf edge and upper slope (maximum 200 m water depth), using different positioning systems and seismic sources. The older analogical profiles were collected between 1985 (data positioning with Loran C system) and 1993 (data positioning with GPS) using the following devices: i) a Uniboom system, recording a sweep of 250 ms with a 500–3000 Hz band pass filter, ii) a 1 kJ Sparker system, recording a sweep of 250 ms with 200–1000 Hz band pass filter, and iii) a 3.5 kHz Sub-Bottom Profiler recording a 125 ms sweep. The analogue seismic records were digitized and transformed to the standard SEGY format using IMAGE2SEGY (Farran, 2008).

2–7 kHz CHIRP and 1 kJ Sparker profiles were collected and DGPS-positioned during four cruises performed between 2010 and 2016. All seismic profiles were integrated in a Kingdom Suite project for the seismic-stratigraphic analysis. In the study area, signal penetration was generally <120 ms for Sparker profiles and reached a maximum of 30 ms for SBP and CHIRP profiles; vertical resolution resulted in the order of several metres for Sparker profiles and sub-metric for SBP and CHIRP profiles. For time-depth conversion of seismic profiles, we used a reference value of 1500 m/s, which is typically used for shallow post-glacial deposits (e.g., Hamilton, 1979; Trincardi et al., 1994). All the data were re-interpreted to ensure consistency among different datasets.

3.3. Post-LGM S2S sediment budget

The S2S budget was calculated by comparing the gross sediment volume (including porosity) produced by the river network and the gross sediment volumes stored on the shelf and coastal plains during the post-LGM interval (last 20 ka, according to the sea-level curve of Lambeck et al., 2011). The volume calculation was also partitioned both in space (Coastal Range, further sub-divided in CRN and CRS, and Santa Eufemia Plain and offshore area, SEP, Fig. 4) and in time, to account for deposition during different phases of the sea-level curve (TST and HST units). In this study, the limit between HST and TST deposits was indirectly constrained at 6.9 ka, based on the correlation of the marine MFS with the stratigraphic surface recording the change from coastal ingression and aggradation to overall coastline progradation in the Santa Eufemia Plain, as reconstructed by Ruello et al. (2017). Our S2S budget does not include the material trapped within the upper part of river valleys or sourced by sea cliff erosion.

3.3.1. Estimation of sediment volumes sourced by rivers

Average long-term uplift rates from late Quaternary palaeoshorelines and marine terraces were used as a proxy for basin-wide denudation rates (Meschis et al., 2022 and reference therein), in turn used to estimate values of mean sediment yield (Table S2; Hinderer et al., 2013) based on the following equation:

$$SY = Dr\,\rho_r \quad (2)$$

where SY (t km^{-2} yr^{-1}) is the sediment yield, Dr (mm/yr) is the total denudation rate, and ρ_r (kg m^{-3}) represents the solid bedrock density.

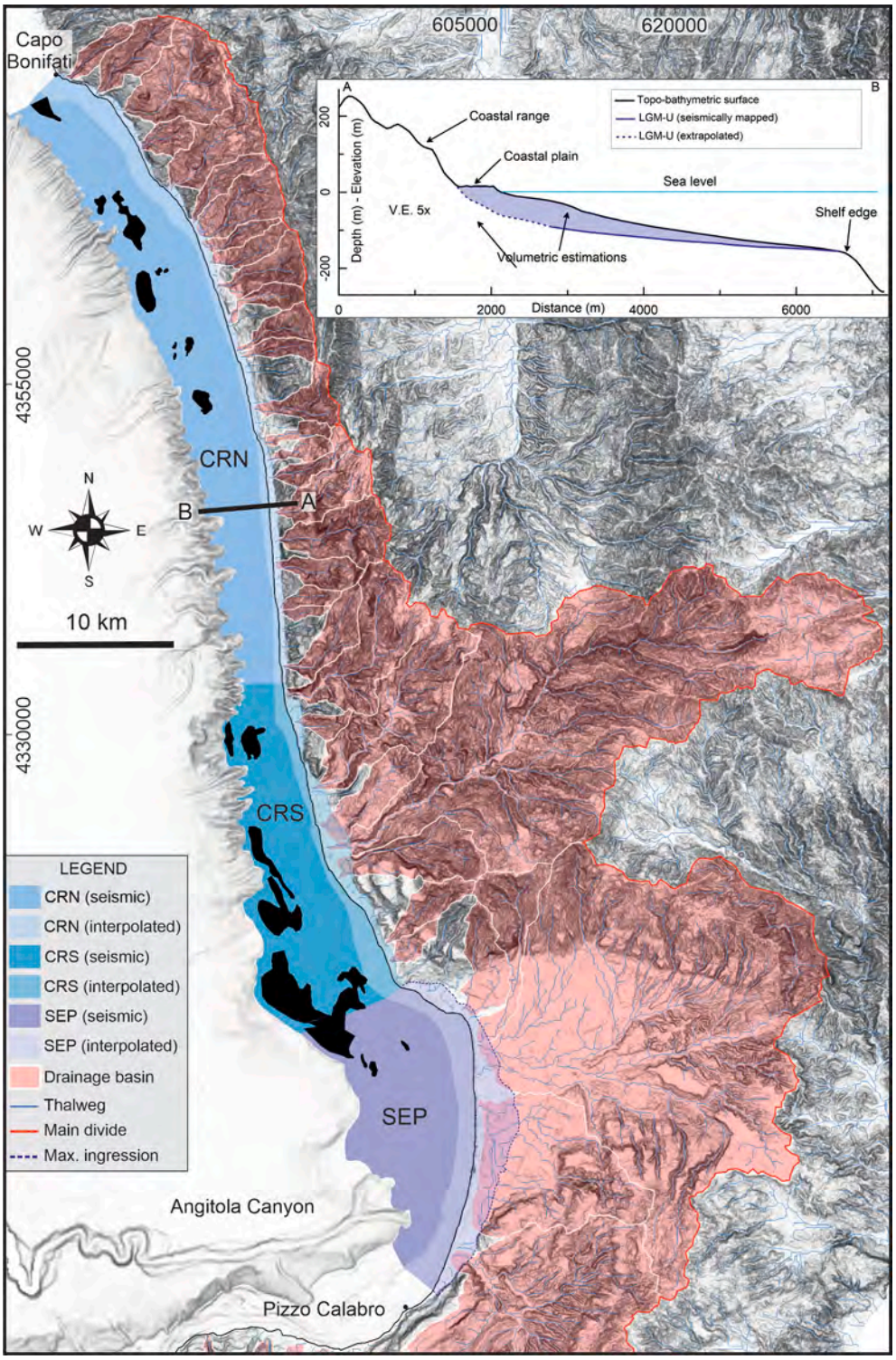

Fig. 4. Shaded relief map (azimuthal light) of the study area, with the indication of the subaerial drainage basins (red polygons delimited by white lines), the divide (thick red line) between fiumara-like rivers (light-blue lines) flowing towards the Tyrrhenian (west) and Ionian Sea (east), and the limit of the marine ingression (dashed blue line) in the SEP reconstructed by Ruello et al. (2018). In the continental shelf, the study area is divided in three sectors: North and South Coastal Range (CRN and CRS, respectively), Santa Eufemia Plain and offshore area (SEP). For each sector, the coloured polygons with variable transparency show the different areas where volumetric estimations were performed using a base surface seismically mapped (middle and outer shelf) or extrapolated for the inner shelf and coastal plain. In the upper right, the profile A-B (located in the main figure) shows the extrapolated geometry of the LGM-U following the trend of the Coastal Range slope and constrained by available boreholes on the coastal plain. (For interpretation of the references to colour in this figure legend, the reader is referred to the web version of this article.)

The basin area (A in km^2) and sediment density (ρ_b in kg m^{-3}) were used to convert the mass into estimates of sediment volume annually produced by a drainage basin (SV in km^3 yr^{-1}; Hinderer, 2001; Hinderer et al., 2013):

$$SV = SY(A/\rho_b) \quad (3)$$

Values of 1500 and 2500 kg m^{-3} were used for sediment and solid bedrock density, respectively. The former is the typical value measured for mixed sediment (Hinderer, 2001; Hinderer et al., 2013; Delaney et al., 2018), whereas the solid bedrock density value is assumed by considering the main lithologies outcropping in the study area; these consist essentially of metamorphic and ophiolitic rocks, locally highly weathered and affected by secondary porosity (e.g., gneiss, micaschists, phyllites; Calcaterra and Parise, 2010).

SY and SV values estimated using Hinderer's approach were also compared with those computed by applying the equations of Milliman and Syvitski (1992), which are based on the empirical relationship between sediment yield and drainage area. For most of the river catchments, the values estimated through the two approaches are comparable (Tables S2 and S3).

3.3.2. Estimation of sediment volumes emplaced on the shelf and coastal plain

The volumetric computation of the material stored on the shelf and coastal plains was carried out by defining the thickness of the HST and TST units as difference between the present-day subaerial/submarine topography and the depth of two key seismo-stratigraphic surfaces, corresponding to the LGM-unconformity (LGM-U) and the maximum flooding surface (MFS). For each unit, the total volume was the sum of three sub-volumes, affected by different uncertainties (Fig. 4 and Table S4). The first sub-volume was computed in the shelf area surveyed by seismic profiles, where the LGM-U and MFS were reliably identified. The second and third sub-volumes were computed for the nearshore area of the shelf (not covered by seismic profiles) and coastal plains, where only scattered stratigraphic information are available. The key stratigraphic surfaces mapped on the middle and outer shelf are thus extrapolated landward based on scattered data and geometric inference on the possible landward trend of each surface. The geometric trend is inferred from stratigraphic logs (ISPRA well catalogue; https://www.isprambiente.gov.it/it/banche-dati/banche-dati-folder/suolo-e-territorio/dati-geognostici-e-geofisici) and limited core data (Ermolli et al., 2018) available inland, on the background of the regional slope gradient of the crystalline units bounding the coastal plain (inset in Fig. 4). In the CR, both TST and HST volumes have been more readily estimated because coastal plains are very narrow, allowing to confidently reconstruct inland extent of the LGM-U and MFS. In the SEP, where the coastal plain is much wider, only the HST volume has been defined, largely based on Holocene stratigraphic data. In this case, the MFS surface has been tentatively traced landward, up to the limit of the transgressive coastline (blue dashed line in Fig. 4) reconstructed by Ermolli et al. (2018), before the onset of coastal progradation associated with HST conditions occurred at 6.9 ka (Ruello et al., 2017).

4. Results

4.1. River and coastal plain morphology

The CRN is drained by 25 short and steep rivers, mainly rectilinear in plan-view (Fig. 5a), with very narrow and V-shaped thalwegs (Fig. 6e). They show an overall concave up profile (Fig. 6b) and steep gradients (~20° on average; Table S1), rapidly attenuating in the narrow (up to 600 m) coastal plain (Fig. 5a).

The CRS is dissected by 8 rivers, among which the Savuto and Oliva rivers show larger drainage areas (Fig. 5b and Table S1), and wider and flat-bottomed thalwegs (Fig. 6e). The longitudinal profile of rivers is generally concave up and regular, locally with some knickpoints (Fig. 6c: LePera and Sorriso-Valvo, 2000). Coastal plains are larger than in the CRN, with a maximum width of ~2 km in the case of the Savuto River (Fig. 5b).

The Angitola and Amato rivers are the main ones among the 5 draining the SEP (Fig. 5c), and are characterized by a large and flat-bottomed thalweg (Fig. 6e). River profiles are usually steeper in the upper reach (with some knickpoints located between 600 and 800 m; Fig. 6d) and became gentle in the middle and lower reaches. Wide alluvial/coastal plains are present, reaching a maximum width of ~5 km in the case of the Amato River (Fig. 5c).

4.2. Basin-scale morphometry and estimation of post-LGM sediment volumes

The CRN domain shows both the largest difference between the minimum and maximum elevations (Fig. 7a) and the highest uplift rates (between 0.5 and 0.9 mm/yr, Fig. 7b); the latter shows an increasing pattern up to catchment 15, followed by a general decrease. Basin-wide *ksn,* basin-averaged slopes, and local relief show an almost regular pattern up to catchment 6, followed by a more scattered pattern with local maxima and minima (Figs. 7c, d, e and Table S1). Precipitation rates are evenly distributed across the CRN, with a slight decrease from north to south (Fig. 7f; Table S1). The river catchments draining the CRN produce an estimated annual sediment volume variable from 2500 to 42,400 m^3 yr^{-1} (Table S2), accounting for a cumulative post-LGM volume of 6.16 km^3 (Table 1).

The CRS domain shows an overall decrease of the difference between minimum and maximum elevation compared to the catchments draining the CRN (Fig. 7a), due to the presence of larger river valleys and coastal plains (Fig. 5b). Uplift rates gradually decrease southwards from 0.5 to 0.3 mm/yr (Fig. 7b; Table S1). Basin-wide *ksn,* basin-averaged slopes, and local relief slope show an overall decrease pattern up to catchment 27, followed by an increase up to catchment 30, with an abrupt minimum at catchment 31 (Figs. 7c, d, e; Table S1). Precipitation values are quite constant and comparable with those in the CRN (Fig. 7f and Table ESM1). The river catchments draining the CRS produce an estimated annual sediment volume ranging from 3500 to 42,500 m^3 yr^{-1} (Table S2), accounting for a cumulative post-LGM volume of 7.76 km^3(Table 1).

The SEP domain shows the minimum difference between minimum and maximum elevations (Fig. 7a) in correspondence of the ~5-km wide alluvial/coastal plain (Fig. 5c), followed by an increase in the southernmost portion of this sector. Uplift rates, basin-wide *ksn*, basin-averaged slope, and local relief values are generally lower than in the CR and they are uniformly distributed over the SEP (Fig. 7b-e and Table S1); precipitation rates are also evenly distributed (Fig. 7f and Table ESM1). The river catchments draining the SEP produce an estimated annual sediment volume ranging from 10.500 to 240,400 m^3 yr^{-1} (Table S2), accounting for a cumulative post-LGM volume of 8.41 km^3(Table 1).

4.3. Morphology of the continental shelf

In the study area, the continental shelf is very narrow (< 1 to 9 km wide), with the shelf break located between 140 and 160 m water depth (Figs. 1 and 5). The shelf has slope gradients varying between 0.5° in the SEP (off the Amato River) and > 2° in the CRS (off Amantea). Aside from the CRN sector encompassed between S. Lucido and Amantea, the morphology of the continental shelf is generally uneven, due to the occurrence of several morphological highs (Fig. 5) associated with the exposure of pre-LGM deposits or build-ups structures (Fig. 3; section 2.3). These morphological highs vary in size, with lengths ranging from few tens of meter to over 1 km, widths from few tens of meters to hundreds of meters, and vertical relief from few meters to several tens of meters. They are mainly concentrated in the CRS, off Capo Suvero (Fig. 5b), while more scattered structures are recognizable in CRN

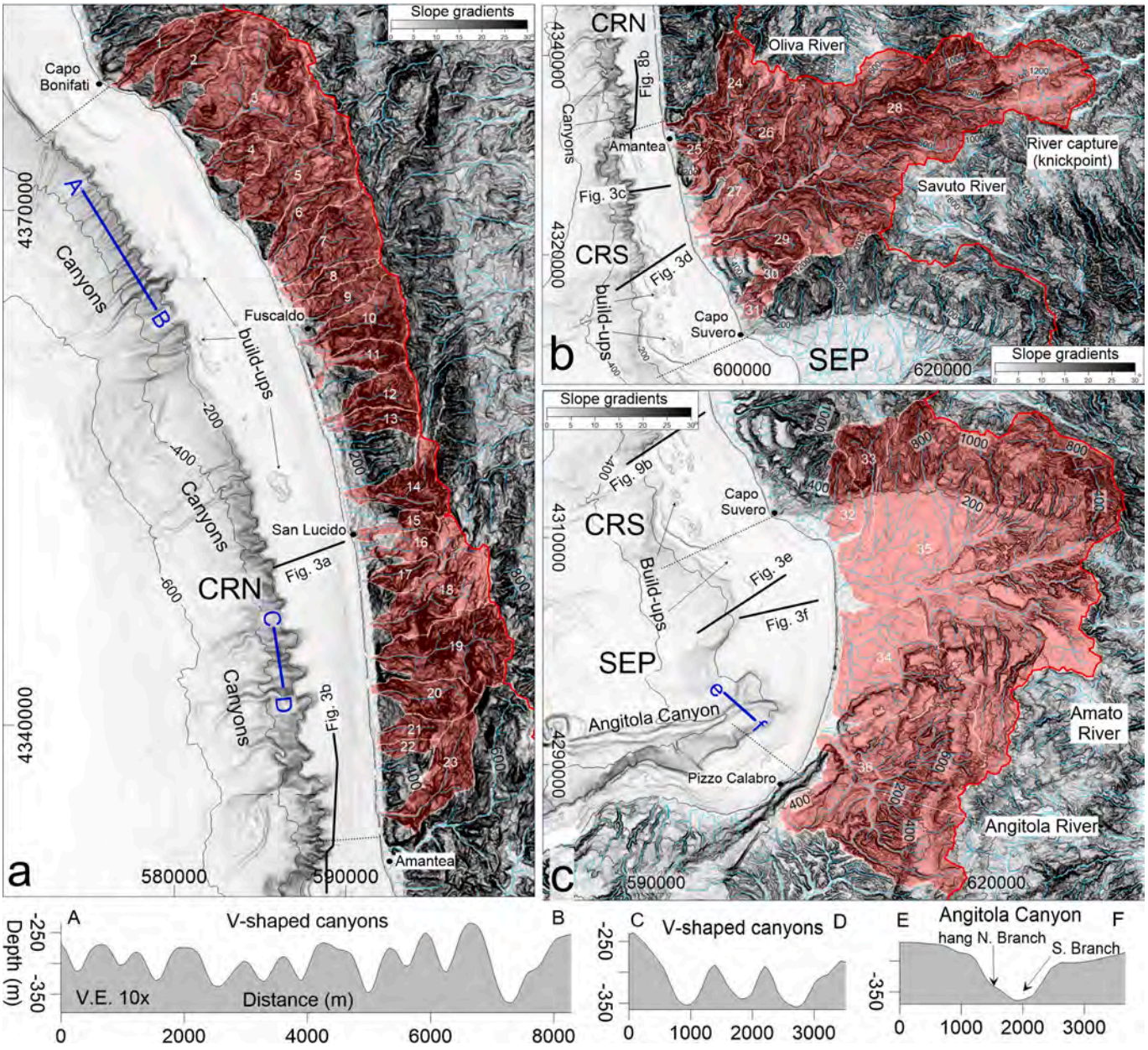

Fig. 5. Slope gradient map of the three sectors (CRN, CRS and SEP in **a, b** and **c**, respectively), with indication of the main morphological features and numbering of the drainage basins here present (see Table S1 for the related morphometric characteristics). Acronyms as in the previous figures. In the lower panels, bathymetric profiles (location in the main figures) showing the cross-section of selected submarine small canyons.

between San Lucido and Fuscaldo (Fig. 5a). Off the river mouths, the shelf is often eroded by a network of narrow gullies, sometimes reaching the shelf break (Fig. 3b; Casalbore, 2024). A dense network of small shelf-indenting canyons is present along the entire Coastal Range, except for a small sector located off Fuscaldo (Figs. 1, 5a and b). Canyons are characterized by a width variable from few to several hundreds of meters; their length ranges from 2 to 10 km. Canyons heads are located between 100 and 150 m water depth, approximately 2.5–5 km far from the coastline, often showing small-scale erosive scars with marked vertical relief. Most canyons are also characterized by a main thalweg, with V-shaped or U-shaped cross-sections (bathymetric profiles in Fig. 5). In the SEP, the shelf is indented by the Angitola Canyon (Figs. 1 and 5c), characterized by a composite head divided into two branches: the northern one is located at about 200 m water depth, 10 km far from the Amato River mouth, and shows an overall smoothed morphology (Fig. 6c). The southern branch is located at about 100 m water depth, 3 km far from the Angitola river mouth, and shows evidence of axial incision in the upper reach. The two branches merge at approximately 350 m water depth, with the northern branch hanging over the southern one, where it forms a scarp of few tens of meters high (profile *E*-F in Fig. 5).

4.4. Isopaches map and stored volumes on the shelf/coastal plain

The isopaches map of post-LGM and HST deposits generally shows a marked decrease of sediment thickness from the inner/middle to the outer shelf, with some exceptions related to the local occurrence of LGM-U irregularities or build-ups structures (black polygons in Fig. 8), acting as obstacle for sedimentary gravity flows or shelf currents, creating small sediment depocenters (Fig. 3d and f).

In the CRN, the shelf is characterized by a main post-LGM depocenter (70–80 ms t.w.t.), which extends 19 km almost continuously and

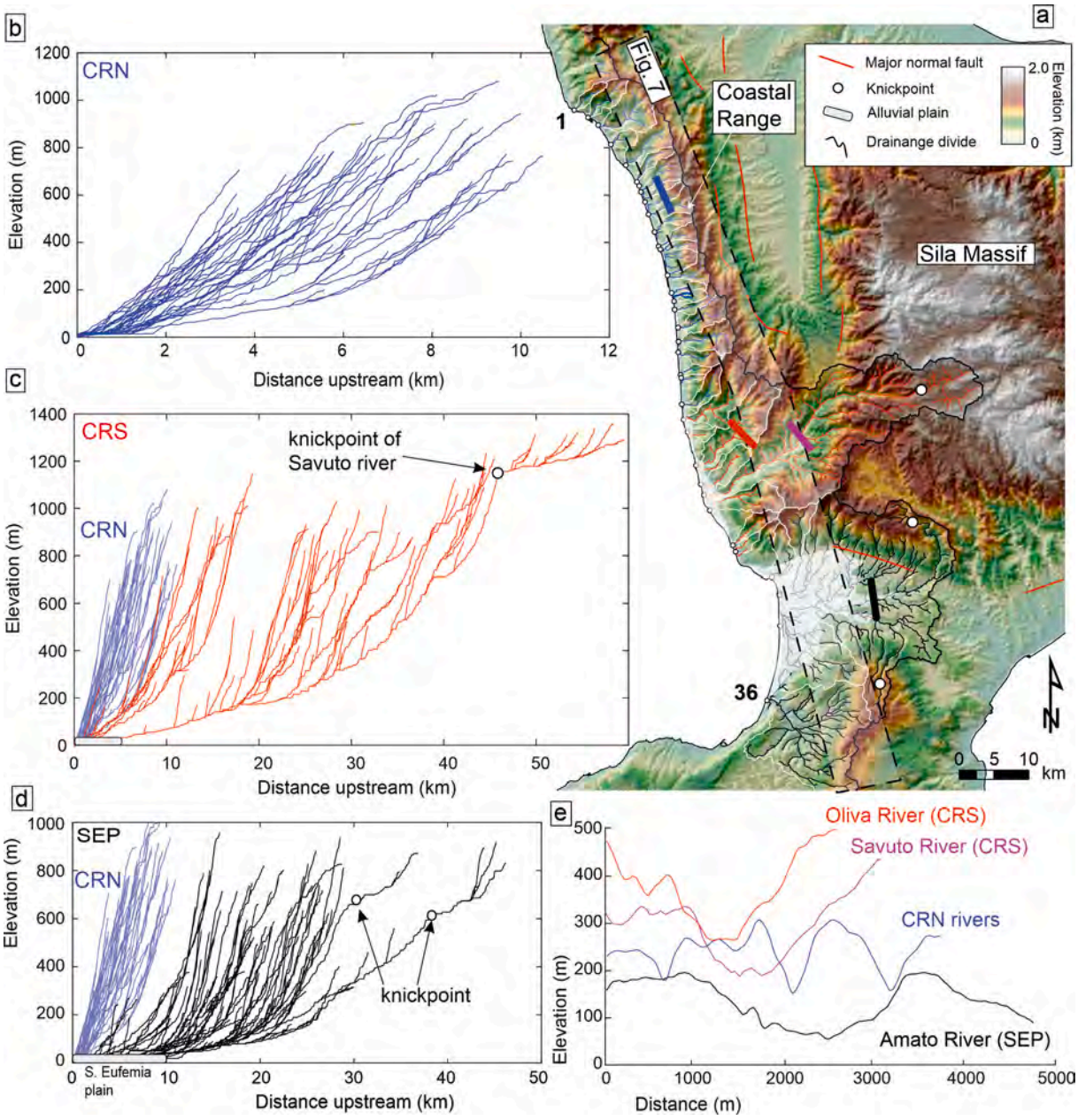

Fig. 6. Topographic map **(a)** and longitudinal river profiles **(b-c-d)** of the CRN (blue lines), CRS (red lines) and SEP rivers (black lines), with indication of the major knickpoints (white point). **e)** Cross-sections of selected river catchments draining the CRN, CRS and SEP. (For interpretation of the references to colour in this figure legend, the reader is referred to the web version of this article.)

subparallel to the coastline between S. Lucido and Amantea (Fig. 8a). Minor depocenters are present in the northern part, off Paola, Fuscaldo and Cetraro. The estimated post-LGM volumes stored on the shelf and coastal plain are 4.86 km^3 and 0,6 km^3 (Table 1), respectively. Greater part of the shelf sediment volume (61%) is attributed to the HST (Fig. 9), which shows spatial distribution not dissimilar from the bulk post-LGM unit (Fig. 8).

In the CRS domain, the shelf is characterized by two post-LGM depocenters (up to 60–70 ms t.w.t.) off the Savuto and Oliva rivers, respectively (Fig. 8a). The southern part of this sector (off Capo Suvero) is characterized by a marked decrease of sediment thickness, with values <10–20 ms (t.w.t.). This area is a morphological high in the isochrone map of LGM-U (Fig. S1a), representing the offshore elongation of Capo Suvero. The estimated post-LGM volumes on the shelf and coastal plain are 2.31 km^3 and 0.59 km^3 (Table 1), respectively. Most of this volume (60%) is contributed by HST unit (Fig. 9), which shows a main depocenter only off the Savuto River (Fig. 8b).

In the SEP, the shelf is characterized by a main post-LGM depocenter (up to 60–70 ms t.w.t.), south of the Amato River mouth (Fig. 8a). Grater part of this area corresponds to a wide depression in the isochrone map of the LGM-U (Fig. S1a). A post-LGM volume of 2.71 km^3 is estimated only for the shelf (Table 1), because of the wide coastal plain and absence of reliable inland stratigraphic data. Most part (63%) of this volume is owned to the HST unit (Fig. 9), which shows a main depocenter centred off the present-day Amato River mouth (Fig. 8b). The estimates for the HST volumes are of 1.7 km^3 and 1.36 km^3 (Table 1) on the shelf and coastal plain (up to the limit of the maximum flooding in Fig. 4), respectively.

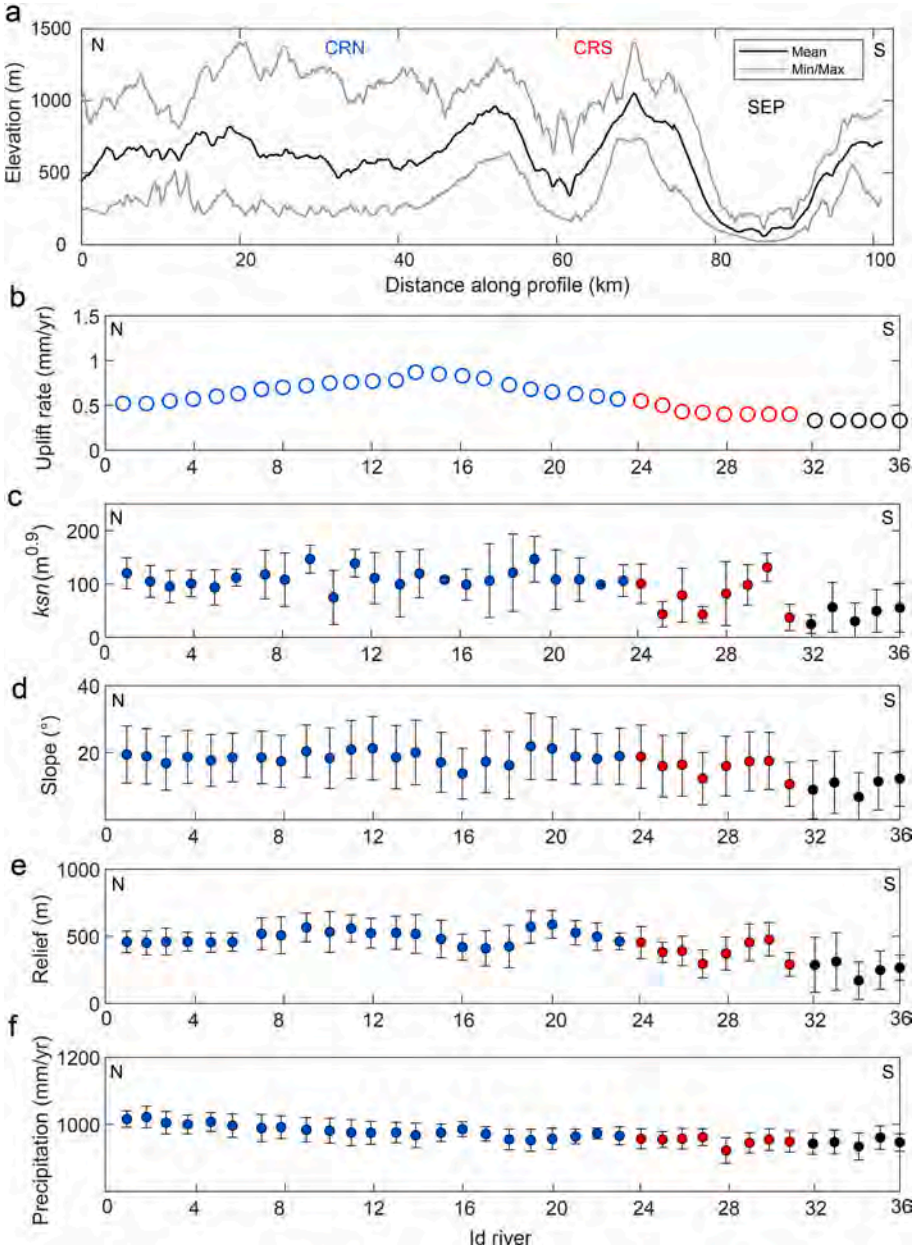

Fig. 7. **(a)** Topographic swath profile along the main divide of the study area (location in Fig. 6a). **(b)** Rates of inferred uplift projected along the selected catchments (Meschis et al., 2022 and reference therein). Basin-averaged **(c)** ksn, **(d)** slope, **(e)** local relief and **(f)** precipitation rate for the river basins.

5. Discussions

5.1. S2S budget along the Calabro-Tyrrhenian continental shelf

The comparison between the post-LGM sediment volumes sourced by rivers and stored on the shelf shows significant differences between the analysed sectors (Table 1 and Fig. 9), possibly resulting from their distinct physiographic settings and the interplay between along- and across-shelf sediment redistribution.

In the CR, the shelf volume corresponds to about half of the sediment volume sourced by rivers (Table 1). A similar percentage has been documented along the Californian Margin (Johnson et al., 2020), which is also characterized by a narrow shelf bordered by coastal mountains. According to Johnson et al. (2020), the sediment loss along the California shelf may be related to off-shelf sediment export by sedimentary gravity flows or resuspension processes during storms; sediment trapping within the river valleys should be also accounted for. A comparable percentage of post-LGM sediment loss has been also documented off the Waipaoa River margin in New Zealand, where it has been mainly attributed to lateral sediment redistribution by shelf-parallel currents (Kuehl et al., 2016 and reference therein). The key role of shelf currents in sediment dispersal (often neglected in many S2S budget estimations) has been described in different cases, evidencing how sediment advection is active as far as tens or hundreds of kilometers away from the source point (e.g., Lu and Fulthorpe, 2004; Cattaneo et al., 2007; Liu et al., 2009; Casalbore et al., 2022).

The CRN shows the highest percentage (~80%) of riverine sediment stored on the shelf. This likely reflects the greater efficiency of sediment supply by linear sources (closely spaced and steep rivers with a narrow coastal plain, Fig. 6b) along the CRN, compared to the point sources (larger rivers with wider coastal plain) present along the CRS and SEP (Figs. 5, 6 and 9). However, part of this volume (especially fine-grained sediments) is likely due to the redistribution of sediments from CRS to CRN by a dominant northward-directed shelf current (Pinardi and

Table 1
Volumetric estimations (km^3) performed for each single sector and divided for post-LGM (20 ka), TST (13.1 ka) and HST (6.9 ka) deposits. The limit between HST and TST deposits has been related to a marked environmental change occurred at 6.9 ka, from coastal ingression and aggradation to an overall coastline progradation, in the SEP (Ruello et al., 2017). This change has been correlated to the variation in shelf architecture observed above a regional reflector, interpreted in this work as the maximum flooding surface (Fig. 3). The blue and light blue columns indicate the stored sediment volume on the shelf and coastal plain, respectively. For more details about the volumetric estimations of the volume stored on the shelf and coastal plains see Table S4. The light brown column indicates the volumes sourced by rivers according to the Hinderer et al. (2013). For more details about the volumetric estimations of the volume sourced by rivers see Table S2. Acronyms as in the previous figures.

Post-LGM	Shelf	Coastal plain	River supply
CRN	4.86	0.6	6.16
CRS	2.31	0.59	7.76
CR (total)	7.17	1.19	13.92
SEP	2.71	n/a	8.41
TST	Shelf	Coastal plain	River supply
CRN	1.91	0.46	4.04
CRS	0.92	0.41	5.08
CR (total)	2.83	0.87	9.12
SEP	1.01	n/a	5.51
HST	Shelf	Coastal plain	River supply
CRN	2.95	0.14	2.12
CRS	1.39	0.18	2.68
CR (total)	4.34	0.32	4.8
SEP	1.7	1.36	2.9

Masetti, 2000). Approximately 10% of the loss volume is stored in the narrow coastal plain (Table 1), while river aggradation can be considered negligible in the CRN because of the steep, narrow, and V-shaped thalwegs that hamper such process (Figs. 5a and 6e). The remaining 10% of the sediment loss (minimum estimation without considering along-shelf redistribution) might result from off-shelf export, favored by the narrow shelf (2–5 km wide) and widespread occurrence of small canyons indenting the shelf edge (Figs. 5 and 9). This off-shelf export would be promoted by the severe storms during the winter months and the torrential regime of the steep rivers as well. In the first case, storm-waves with maximum significant waves up to 9 m and wave periods of 5–6 s (Foti et al., 2022) are considered the main mechanism for sediment resuspension over the shelf, as also suggested for other narrow shelves located along the Palomares margin in southern Iberia (Puig et al., 2017) and Eel margin in California (Puig et al., 2003). In the second case, these rivers are highly prone to sudden and catastrophic flash-flood events capable of transporting significant sediment loads into the marine environment (Sabato and Tropeano, 2004; Clementucci et al., 2022a). This phenomenon often leads to the frequent generation of hyperpycnal flows, as evidenced by recent events in the Messina Strait (Casalbore et al., 2011) and at Bagnara Calabra (Alberico et al., 2022). This also suggests a high riverine OC preservation in the shelf depocenters because of the rapid, event-driven accumulation of sediment (Blair and Aller, 2012). In the study area, flash-floods events and sea storms often temporally coincide, due to the interplay between the prevalent westerly direction of the wind and the eastward topographic barrier created by the Coastal Range (Foti et al., 2022). This dynamic interaction has the potential of amplifying off-shelf export and lateral advection of the riverine plumes. Evidence of this off-shelf export is provided by i) the network of small gullies associated with prodeltaic systems (Fig. 3b), whose formation can be related to flash-flood generated hyperpycnal flows (e.g., Casalbore, 2024); ii) the erosive morphologies with marked morphological relief identified at some canyon heads, possibly indicating recent sedimentary dynamics; iii) the axial incision that characterizes the course of some canyons in the upper slope, as evidenced by their V-shaped cross-section (profiles a-b and c-d in Fig. 5a) and lack of relevant sedimentary infilling along their thalweg (Fig. 3b); iv) the homogenous distribution of the 2 m-thick Holocene fine-grained deposit recognized in the facing slope and basin (Trincardi et al., 1995).

In the CRS, only 30% of the sediment sourced by rivers is stored on the shelf, indicating a larger loss, despite the estimated off-shelf export should be comparable to the CRN, due to the similar spatial distribution and morphological characteristics of the shelf-identing canyons (Figs. 5b and 9). Therefore, a significant portion of the sediment loss can be attributed both to the trapping of riverine material within the larger coastal plains and broader river valleys present in this area (Figs. 5b and 9), and the along-shelf redistribution of sediment due to the dominant northward-directed shelf current. In the first case, the post-LGM sediment volume stored on the coastal plains is only 8% of the volume sourced by rivers along the CRS (Table 1). A similar or lower percentage can be inferred for river aggradation, mostly corresponding to the flat-bottomed thalweg area along the river courses (Figs. 5b, 6e and 9), which has a cumulative value slightly greater than the coastal plain, but with a lower sediment thickness. This means that a significant percentage of sediment is redistributed from CRS to CRN by the northward-directed shelf current, as also suggested by the elongated and shore parallel post-LGM and HST depocenters along the CRN (Fig. 8a) and the TST vs HST S2S budgets as well. In particular, the HST budget shows a shelf volume larger than the sourced volume in the CRN (Table 1), clearly pointing out a sediment supply from the CRS. This northward sediment transport is supported both by the general north deflection of modern riverine plumes, evidenced by recent satellite images (Copernicus: Sentinel 2), and by the asymmetric accumulation of the HST unit around the build-ups observed on seismic profiles, likely acting as an obstacle for the current flow. This sediment supply from CRS to CRN also suggests that the 10% value for the off-shelf export in the CRN (and consequently in the CRS) is underestimated. It is also noteworthy that the amount of off-shelf export would have been significantly higher during the post-LGM transgression when the coastline was closer to the shelf edge, as demonstrated by the much lower (almost 3 times) storage percentage of shelf sediment during the transgression compared with the highstand condition (Table 1 and Fig. 9).

A different scenario can be envisaged for the SEP, where the post-LGM budget also shows a low percentage (32%) of stored volume in the shelf, reaching a minimum value of 18% for the TST unit. Despite part of this sediment loss can be attributed to sediment redistribution due to northward-directed shelf current, in this sector a key role is likely played the physiographic setting, characterized by the development of a significantly wider coastal plain (especially in comparison to the CR), which acted as a sediment trap for riverine sediment. This interpretation is supported by the higher percentage (47%) of HST sediment stored on the SEP coastal plain with respect to the CR (7%). Unfortunately, we cannot extend the same consideration to the TST unit, because reliable stratigraphic and geophysical constraints on the coastal plain are lacking for the pre-Holocene interval. However, it is likely that a paleo-valley linked with the Amato River was present, representing a main sediment trap for riverine sediments, as for instance observed in the nearby Metaponto Plain (Tropeano et al., 2013). A network of small fiumara-like rivers currently cuts through the upper stratigraphic succession of the Metaponto coastal plain. Differently, a few large and up to 60 m deep river-valleys were present during the last glacial interval; these were totally filled during the subsequent sea level rise, determining a significant lateral variability in thickness of the post-LGM deposits (Tropeano et al., 2013). Based on the similarity of the geological setting, we propose that river aggradation within the Amato paleo-river valley and,

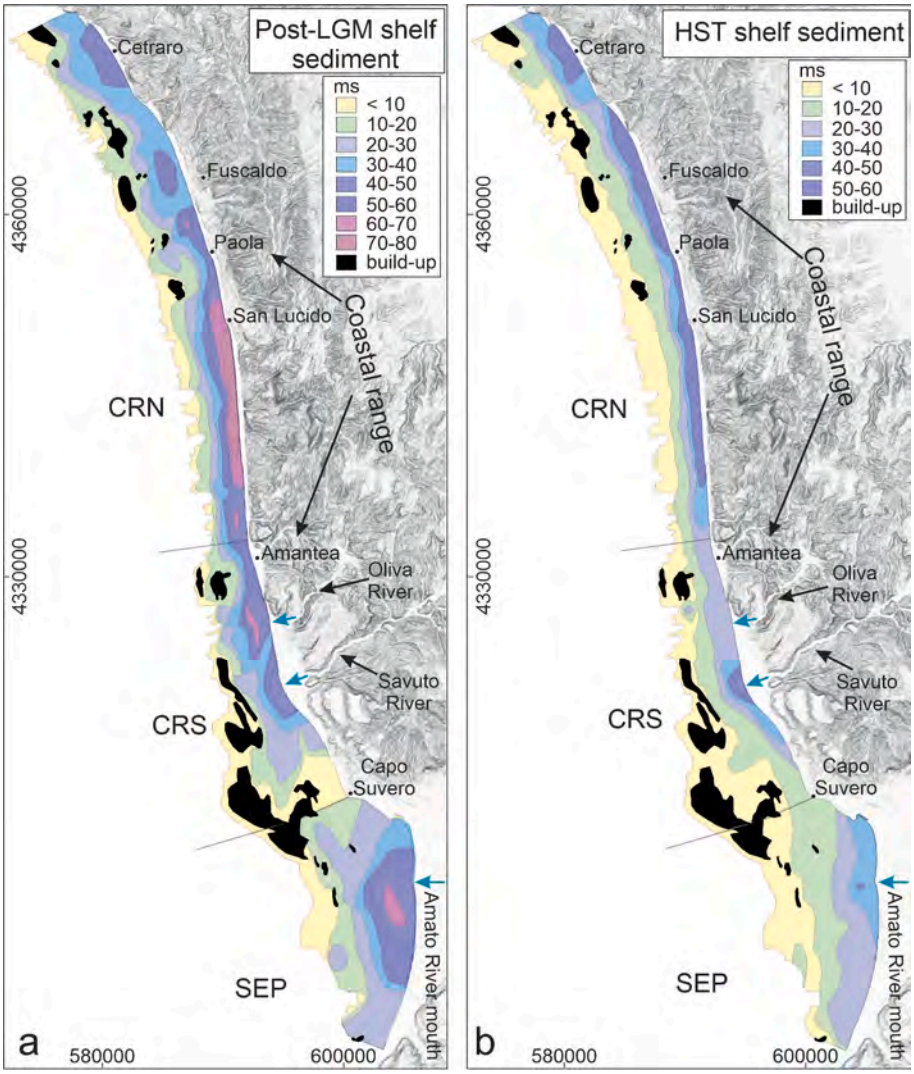

Fig. 8. Isopach map of the post-LGM (a) and HST (b) deposits in the study area (ms: milliseconds in T.W.T.: two-way travel time); the black polygons indicate exposure of pre-LGM deposits/build-up structures.

more generally, on the wide SEP coastal plain, coupled with the off-shelf export (mainly during the transgression) at the Angitola Canyon, can be considered the main processes responsible for the low preservation of TST deposits (18%) in this shelf sector.

5.2. Advantages and limitations of the approach used for estimating the post-LGM S2S budget along the Calabro-Tyrrhenian shelf

The main advantage of the proposed approach is the possibility to re-exploit high-resolution seismic data, previously collected on shelf sectors for other purposes, aimed at providing a first estimation of the S2S shelf budget at the scale of the last hemieustatic cycle. Moreover, when combined with the reconstruction of the Upper-Pleistocene shelf architecture, this post-LGM volumetric estimation can also give some hints for S2S studies at the scale of a complete glacio-eustatic cycle from the source area to the final sink, i.e., the deep basin. It is important to consider that shelf storage can significantly change in relation to the different tectonic settings of the margin (i.e., uplifting or subsiding margins; for details see Appendix a). In the case of uplifting margin (such as the Calabro-Tyrrhenian margin, Fig. S2b), the shelf mainly acts as a temporary storage for riverine sediments, because these are never significantly buried below wave-base erosion of lowstand intervals during 100 ka glacio-eustatic cycles (e.g., Hernández-Molina et al., 2000; Lobo and Ridente, 2014). In contrast, shelf sequences are progressively buried and preserved on subsiding margins during successive sea level cycles (Fig. S2c; Rabineau et al., 2005, Jouet et al., 2008; Ridente, 2016).

One of the main limitations in estimating the post-LGM shelf budget has been the lack of data from nearshore areas, largely inaccessible during surveys because restricted to navigation. In addition, geophysical data acquired in navigable shallow waters are of low quality and typically affected by seismic artifacts (e.g., seabed multiple at shallow depths or acoustic masking due to the presence of gas-charged sediment). In these cases, key stratigraphic surfaces are inferred based on the extrapolation of data from adjacent areas. Similar problems affect sediment budget estimation in the coastal plains where reliable stratigraphic reconstructions are limited by the poor density of ground truthing and chronostratigraphic data. These issues differently impact our results, with effects that vary along the coast between two end-member settings: the SEP and the CRN. In the SEP, the wider shelf and coastal plain, coupled with the limited stratigraphic constraints in this area, has hindered the accuracy of the estimated post-glacial S2S budget, only allowing a rough estimation for the HST unit. On the contrary, the CRN is characterized by mountainous areas close to the coast and narrow coastal plains, limiting the extent of data extrapolation and reducing the resulting uncertainties (Fig. 4). Some obstacles in

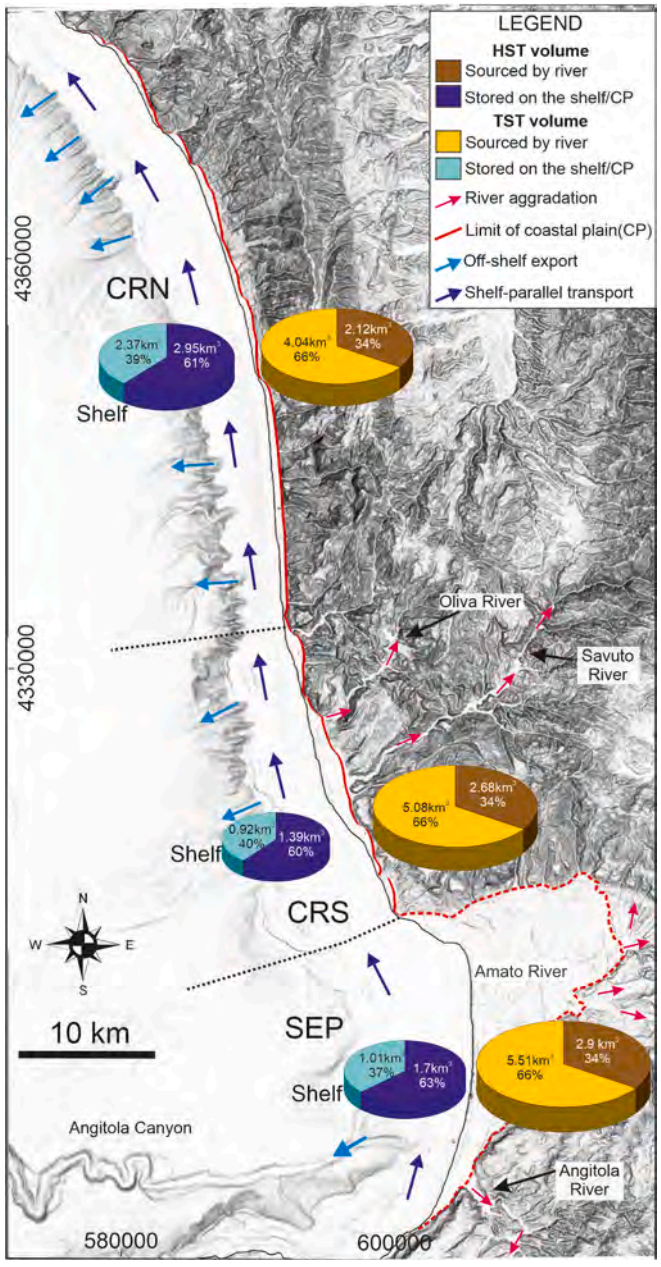

Fig. 9. Sketch showing the comparison between the gross volumes of post-LGM sediments sourced by the rivers and those stored on the shelf within the three different sectors identified in the study area (CRN, CRS and SEP); volumes are also partitioned between HST and TST units.

defining sediment volumes also come from fluid-charged sediments or even from shallow pre-LGM deposits/build-up structures (especially in the CRS) that strongly absorbs the seismic signal, hindering deeper reflections. These problems have been lessened by the density of seismic profiles with different resolution and penetration, which allowed a confident interpolation of the LGM-U and MFS surfaces in these areas. Differently, the lack of reliable chronological constraints represents a main problem for the partitioning of the TST and HST units within the post-LGM volume. These units were defined through the identification of two key surfaces on seismic profiles, i.e. the LGM-U and MFS surface. Whereas the LGM-U erosional truncation at the base of the TST is evident on seismic profiles, the identification of the MFS is less unambiguous. In the study area, the MFS has been tentatively correlated with a surface constrained at 6.9 ka BP in the SEP coastal plain and marking the transition from coastal ingression and aggradation to overall coastline progradation (Ruello et al., 2017). The difference with the age of the MFS in other margins, usually around 5.5–6 ka BP (Correggiari et al., 2001; Ridente and Trincardi, 2005), likely reflects the varied response of marine and fluvial sedimentary systems in different settings.

Regarding the estimated volume sourced by rivers, our assumption that denudation rates are proportional to the rapid uplift rates of this area is reasonable, especially when averaged for the entire post-LGM period. The rivers in Calabria are well described by the stream power law, as the variation of channel steepness and basin-wide denudation rates often mirrors the spatial variation of the local and regional tectonic uplift (Olivetti et al., 2012; Cyr et al., 2014; Roda-Boluda et al., 2019; Clementucci et al., 2024). Cyr et al. (2010) and Clementucci et al. (2024) observed a good correlation between ^{10}Be-derived denudation rates, marine terraces and vertical incisions (i.e., rock uplift rates), arguing that southern Calabria topography is close to dynamic equilibrium state, where erosion and uplift are balanced. Goswami et al. (2017) also demonstrated, in the nearby Messina Strait, a positive relationship between the average long-term uplift rates and catchment-wide average erosion rates with short-term landslide-based sediment yields, showing that they generally fall in the same range of values. On the other hand, our morphometric analysis of river catchments has evidenced the presence of knickpoints along some river courses, which may separate portions of the landscape eroding at different rates (Figs. 6c and d). These different erosion rates across the same basin would lead to a possible overestimation of the computed supplied sediment. At shorter-terms, denudation rates can depend on different factors, such as bedrock lithologies, precipitation rates, vegetation cover, and landslide activity. In Calabria, the role of lithology has been addressed by several authors (e.g., Ibbeken and Schleyer, 2013; LePera and Critelli, 1997; Cyr et al., 2014), suggesting an overall uniform distribution of rock resistance (Istituto Superiore per la Protezione e la Ricerca Ambientale (ISPRA), 2009). The same can be applied to precipitation rates, which are evenly distributed across the study area (Table S1; Brunetti et al., 2012). However, this assumption is valid for present-day conditions, while variations in precipitation rates and vegetation cover during the last 20 ka cannot be estimated based on available data.

Finally, in an active tectonic setting such as the northern Calabria, landslides can play an important role in the erosional dynamics, leading to a non-linear relationship between channel steepness and denudation rates (Ouimet et al., 2009). This can cause an underestimation of sediment volumes sourced onshore (e.g., hillslope sediment storage on landslides), as observed in southern Calabria (Roda-Boluda et al., 2019). However, this process is significant only during shorter intervals (i.e., a few millennia at maximum according to Roda-Boluda et al., 2019) than those covered by the deposition of the HST (6–7 ka) and TST (13–14 ka).

6. Conclusions

The post-LGM S2S budget conducted on the 90 km long Calabro-Tyrrhenian shelf enabled us to constrain the role of multiple (geomorphic, sedimentary, oceanographic) factors controlling the delivery and accumulation of sediment along a narrow and tectonically controlled shelf.

A first-order factor controlling the storage capacity of the shelf during the post-LGM is the geomorphic setting of the margin. Mountainous areas close to the coast, drained by aligned sources of short and steep rivers with torrential regime, and characterized by narrow coastal plains, show a greater efficiency in supply sediment to the shelf in comparison to wider coastal plains drained by larger rivers. In the latter areas, sediments are mostly trapped in river thalweg and coastal plain before reaching the sea, especially during the transgression. This is suggested by the S2S budget computed for the shelf facing the Coastal Range, characterized by a higher percentage of storage (~50% for the post-LGM and up to 90% for the HST unit) compared to that estimated off the 5-km wide Santa Eufemia coastal plain (only ~30% for the post-LGM). Our analysis also highlighted the significant role of along-shelf

sediment redistribution by northward-directed shelf currents, leading to significant volumetric differences between adjacent sectors that share similar geomorphic conditions, such as those observed in the southern and northern parts of the Coastal Range. This highlights the importance of defining along-shelf sediment redistribution in regional S2S studies, which can be particularly significant at the local scale. In the study area, a significant sediment loss (at least 10% when averaged over the entire post-LGM period) has been attributed to the off-shelf export through a network of shelf-indenting canyons, which appear to be geographically linked to the drainage network inland. Specifically, this off-shelf export is possibly favored by the interaction between sediment resuspension from westerly, energetic storms and flash-flood events that commonly characterize the short and steep rivers. This sediment loss was probably higher during the initial stages of transgression, when the coastline and river mouths were closer to the shelf edge. It likely decreased over time, reaching the minimum when the sea level nearly reached its present-day position, as demonstrated by different partitioning of the S2S budgets between TST and HST units.

In general, this S2S budget should be considered as a preliminary step towards a more detailed S2S study, which would require the acquisition of additional geophysical and stratigraphic data, as well as the use of tracers to further validate the main findings of this study. However, it is important to emphasize the relevance of such cost-effective approaches by exploiting previously collected data to provide a broad overview of the main sedimentary processes controlling the sediment delivery and dispersal on the shelf at a regional scale. This can also provide insights for better understanding the role of the shelf as temporary storage for sediment within a more comprehensive S2S study spanning from the source area to the deep marine basin.

Supplementary data to this article can be found online at https://doi.org/10.1016/j.earscirev.2024.104815.

CrediT authorship contribution statement

Conceptualization: DC, EM, DR; Writing – original draft, DC, EM, DR, RC; Writing - review & editing: DR, DC, EM, RC; FLC; Data curation, formal analysis and methodology: DC, EM, DR, RC; Visualization: DC, EM, DR, RC, Resources and funding acquisition: FLC.

Declaration of competing interest

The authors declare that they have no known competing financial interests or personal relationships that could have appeared to influence the work reported in this paper.

Data availabilityThe bathymetric data are downloadable both by the EMODNET website (https://emodnet.ec.europa.eu/en/bathymetry) and a public server of the Department of Civil Protection in Italy (https://github.com/pcm-dpc/MaGIC/tree/master/MaGIC-1). The seismic data are downloadable upon request by mail to the authors. The morphometric and volumetric data are in the tables of the manuscript and in the electronic supplementary material.

The bathymetric data are downloadable both by the EMODNET website (https://emodnet.ec.europa.eu/en/bathymetry) and a public server of the Department of Civil Protection in Italy (https://github.com/pcm-dpc/MaGIC/tree/master/MaGIC-1). The seismic data are downloadable upon request by mail to the authors. The morphometric and volumetric data are in the tables of the manuscript and in the electronic supplementary material.

Acknowledgements

Crew along with students and researchers participating to the different oceanographic cruises are greatly acknowledged. In particular, a special thank is due to Dr. Francesco Falese that organized the database archive of the seismic profiles used in this paper. The first author also acknowledges the funding provided by “Progetto di Ateneo 2021 and 2022” (P.I. Daniele Casalbore) of University of Rome Sapienza. Global Mapper and IHS Kingdom suite are acknowledged and used to perform morphologic and seismic interpretation. Two anonymous reviewers and the guest editor Stephan J. Jorry are also gratefully acknowledged for their careful revisions that largely improved the quality of the paper.

References

Alberico, I., Casalbore, D., Pelosi, N., Tonielli, R., Calidonna, C., Dominici, R., De Rosa, R., 2022. Remote Sensing and Field Survey Data Integration to Investigate on the Evolution of the Coastal Area: the Case Study of Bagnara Calabra (Southern Italy). Remote Sens. 14 (10), 2459.

Allen, P., 2008. From landscapes into geological history. Nature 451 (7176), 274–276.

Antonioli, F., Ferranti, L., Lambeck, K., Kershaw, S., Verrubbi, V., Dai Pra, G., 2006. Late Pleistocene to Holocene record of changing uplift rates in southern Calabria and northeastern Sicily (southern Italy, Central Mediterranean Sea). Tectonophysics 422 (1–4), 23–40.

Ballato, P., Strecker, M.R., 2014. Assessing tectonic and climatic causal mechanisms in foreland-basin stratal architecture: insights from the Alborz Mountains, northern Iran. Earth Surf. Process. Landf. 39 (1), 110–125.

Blair, N.E., Aller, R.C., 2012. The fate of terrestrial organic carbon in the marine environment. Annu. Rev. Mar. Sci. 4, 401–423.

Blum, M.D., Womack, J.H., 2009. Climate change, sea-level change, and fluvial sediment supply to Deepwater systems. In: Kneller, B., Martinsen, O.J., McCaffrey, B. (Eds.), External Controls on Deep Water Depositional Systems: Climate, Sea-Level, and Sediment Flux, vol. 92. SEPM, Special Publication, pp. 15–39.

Brunetti, M., Caloiero, T., Coscarelli, R., Gulla, G., Nanni, T., Simolo, C., 2012. Precipitation variability and change in the Calabria region (Italy) from a high-resolution daily dataset. Int. J. Climatol. 32 (1), 57–73.

Brutto, F., Muto, F., Loreto, M.F., De Paola, N., Tripodi, V., Critelli, S., Facchin, L., 2016. The Neogene-Quaternary geodynamic evolution of the central Calabrian Arc: a case study from the western Catanzaro Trough basin. J. Geodyn. 102, 95–114.

Calcaterra, D., Parise, M., 2010. Weathering in the crystalline rocks of Calabria, Italy, and relationships to landslides. Geol. Soc., London, Eng. Geol. Spe. Publicat. 23 (1), 105–130.

Casalbore, et al., 2024. Geohazard Features of the Tyrrhenian Calabria. J. Maps. https://doi.org/10.1080/17445647.2024.2347897.

Casalbore, D., Chiocci, F.L., Scarascia Mugnozza, G., Tommasi, P., Sposato, A., 2011. Flash-flood hyperpycnal flows generating shallow-water landslides at Fiumara mouths in Western Messina Strait (Italy). Mar. Geophys. Res. 32, 257–271.

Casalbore, D., Conforti, A., Budillon, F., Martorelli, E., Morelli, E., Pierdomenico, M., Chiocci, F.L., 2024. Geohazard features of the Tyrrhenian Calabria. J. Maps 20 (1). https://doi.org/10.1080/17445647.2024.2347897.

Cattaneo, A., Trincardi, F., Asioli, A., Correggiari, A., 2007. The Western Adriatic shelf clinoform: energy-limited bottomset. Cont. Shelf Res. 27 (3–4), 506–525.

Catuneanu, O., Abreu, V., Bhattacharya, J.P., Blum, M.D., Dalrymple, R.W., Eriksson, P. G., Fielding, C.R., Fisher, W.L., Galloway, W.E., Gibling, M.R., Giles, K.A., Holbrook, J.M., Jordan, R., Kendall, C.G.S.C., Macurda, B., Martinsen, O.J., Miall, A. D., Neal, J.E., Nummedal, D., Pomar, L., Posamentier, H.W., Pratt, B.R., Sarg, J.F., Shanley, K.W., Steel, R.J., Strasser, A., Tucker, M.E., Winker, C., 2009. Towards the standardization of sequence stratigraphy. Earth Sci. Rev. 92 (1–2), 1–33.

Chiocci, F.L., D'angelo, S., Orlando, L., Pantaleone, A., 1989. Evolution of the Holocene shelf sedimentation defined by high resolution seismic stratigraphy and sequence analysis (Calabro-Tyrrhenian continental shelf). Mem. Soc. Geol. Ital. 48, 359–380.

Clementucci, R., Lafosse, M., Casalbore, D., Ridente, D., d'Acremont, E., Rabaute, A., Chiocci, F., Gorini, C., 2022a. Common origin of coexisting sediment undulations and gullies? Insights from two modern Mediterranean prodeltas (southern Italy and northern Morocco). Geomorphology 402, 108133.

Clementucci, R., Ballato, P., Siame, L.L., Faccenna, C., Yaaqoub, A., Essaifi, A., et al., 2022b. Lithological control on topographic relief evolution in a slow tectonic setting (Anti-Atlas, Morocco). Earth Planet. Sci. Lett. 596.

Clementucci, R., Ballato, P., Siame, L.L., Faccenna, C., Racano, S., Torreti, G., et al., 2023. Transient response to changes in uplift rates in the northern Atlas-Meseta system (Morocco). Geomorphology 108765.

Clementucci, R., Lanari, R., Faccenna, C., Crosetto, S., Reitano, R., Zoppis, G., Ballato, P., 2024. Morpho-tectonic evolution of southern Apennines: Insights from Pollino range and surrounding intermountain basins. Tectonics. https://doi.org/10.1029/2023TC008002.

Correggiari, A., Trincardi, F., Langone, L., Roveri, M., 2001. Styles of failure in late Holocene highstand prodelta wedges on the Adriatic shelf. J. Sediment. Res. 71 (2), 218–236.

Cyr, A.J., Granger, D.E., Olivetti, V., Molin, P., 2010. Quantifying rock uplift rates using channel steepness and cosmogenic nuclide–determined erosion rates: examples from northern and southern Italy. Lithosphere 2 (3), 188–198.

Cyr, A.J., Granger, D.E., Olivetti, V., Molin, P., 2014. Distinguishing between tectonic and lithologic controls on bedrock channel longitudinal profiles using cosmogenic 10Be erosion rates and channel steepness index. Geomorphology 209, 27–38.

Delaney, I., Bauder, A., Werder, M.A., Farinotti, D., 2018. Regional and annual variability in subglacial sediment transport by water for two glaciers in the Swiss Alps. Front. Earth Sci. 6, 175.
DISS Working Group, 2021. Database of Individual Seismogenic Sources (DISS), Version 3.3.0: A Compilation of Potential Sources for Earthquakes Larger Than M 5.5 in Italy and Surrounding Areas. United States: Istituto Nazionale di Geofisica e Vulcanologia. https://doi.org/10.13127/diss3.3.0.
Doglioni, C., Harabaglia, P., Martinelli, G., Mongelli, F., Zito, G., 1996. A geodynamic model of the Southern Apennines accretionary prism. Terra Nova 8 (6), 540–547.
Duvall, A., Kirby, E., Burbank, D., 2004. Tectonic and lithologic controls on bedrock channel profiles and processes in coastal California. J. Geophys. Res. Earth 109 (F3).
Ermolli, E.R., Ruello, M.R., Cicala, L., Di Lorenzo, H., Molisso, F., Pacciarelli, M., 2018. An 8300-yr record of environmental and cultural changes in the Sant'Eufemia Plain (Calabria, Italy). Quat. Int. 483, 39–56.
Faccenna, C., Molin, P., Orecchio, B., Olivetti, V., Bellier, O., Funiciello, F., Billi, A., 2011. Topography of the Calabria subduction zone (southern Italy): Clues for the origin of Mt. Etna. Tecton. 30 (1).
Farran, M.L., 2008. IMAGE2SEGY: Una aplicación informática para la conversión de imágenes de perfiles sísmicos a ficheros en formato SEG Y. Geo-Temas 10, 1215–1218.
Flint, J.J., 1974. Stream gradient as a function of order, magnitude, and discharge. Water Resour. Res. 10 (5), 969–973.
Forte, A.M., Whipple, K.X., 2019. Short communication: the Topographic Analysis Kit (TAK) for TopoToolbox. Earth Surf. Dyn. 7 (1), 87–95.
Foti, G., Barbaro, G., Besio, G., Barillà, G.C., Mancuso, P., Puntorieri, P., 2022. Wave Climate along Calabrian Coasts. Climate 10 (6), 80.
Gamberi, F., Marani, M., 2006. Hinterland geology and continental margin growth: the case of the Gioia Basin (southeastern Tyrrhenian Sea). Geol. Soc. Lond. Spec. Publ. 262 (1), 349–363.
Goswami, R., Mitchell, N.C., Brocklehurst, S.H., Argnani, A., 2017. Linking subaerial erosion with submarine geomorphology in the western Ionian Sea (south of the Messina Strait), Italy. Basin Res. 29, 641–658.
Hamilton, E.L., 1979. Sound velocity gradients in marine sediments. J. Acoust. Soc. Am. 65 (4), 909–922.
Helland-Hansen, W., Martinsen, O.J., 1996. Shoreline trajectories and sequences; description of variable depositional-dip scenarios. J. Sediment. Res. 66 (4), 670–688.
Helland-Hansen, W., Sømme, T.O., Martinsen, O.J., Lunt, I., Thurmond, J., 2016. Deciphering Earth's natural hourglasses: perspectives on source-to-sink analysis. J. Sediment. Res. 86 (9), 1008–1033.
Hernández-Molina, F.J., Somoza, L., Lobo, F., 2000. Seismic stratigraphy of the Gulf of Cádiz continental shelf: a model for late Quaternary very high-resolution sequence stratigraphy and response to sea-level fall. In: Hunt, D., Gawthorpe, R.L.G. (Eds.), Sedimentary Responses to Forced Regressions, 172. Geol. Soc. Lond. Spec. Publ, pp. 329–362.
Hijmans, R.J., Cameron, S.E., Parra, J.L., Jones, P.G., Jarvis, A., 2005. Very high resolution interpolated climate surfaces for global land areas. Int. J. Climatol. 25 (15), 1965–1978.
Hinderer, M., 2001. Late Quaternary denudation of the Alps, valley and lake fillings and modern river loads. Geodin. Acta 14 (4), 231–263.
Hinderer, M., Kastowski, M., Kamelger, A., Bartolini, C., Schlunegger, F., 2013. River loads and modern denudation of the Alps—a review. Earth Sci. Rev. 118, 11–44.
Hunt, D., Tucker, M.E., 1992. Stranded parasequences and the forced regressive wedge systems tract: deposition during base-level'fall. Sediment. Geol. 81 (1–2), 1–9.
Ibbeken, H., Schleyer, R., 2013. Source and Sediment: A Case Study of Provenance and Mass Balance at an Active Plate Margin (Calabria, Southern Italy). Springer Science & Business Media.
Ietto, F., Cantasano, N., Pellicone, G., 2018. A new coastal erosion risk assessment indicator: Application to the Calabria Tyrrhenian Littoral (southern Italy). Environ. Process. 5, 201–223.
Istituto Superiore per la Protezione e la Ricerca Ambientale (ISPRA), 2009. Geological Map of Italy. 1:500 000 scale. Accessed through the OneGeology Portal. http://portal.onegeology.org.
Johnson, S.Y., Beeson, J.W., Watt, J.T., Sliter, R.W., Papesh, A.G., 2020. Controls on sediment distribution in the coastal zone of the Central California transform continental margin, USA. Mar. Geol. 420, 106085.
Jouet, G., Hutton, E.W.H., Syvitski, J.P.M., Berné, S., 2008. Response of the Rhône deltaic margin to loading and subsidence during the last climatic cycle. Comput. Geosci. 34 (10), 1338–1357.
Kirby, E., Whipple, K.X., 2012. Expression of active tectonics in erosional landscapes. J. Struct. Geol. 44, 54–75.
Kuehl, S.A., Alexander, C.R., Blair, N.E., Harris, C.K., Marsaglia, K.M., Ogston, A.S., Walsh, J.P., 2016. A source-to-sink perspective of the Waipaoa River margin. Earth Sci. Rev. 153, 301–334.
Lambeck, K., Antonioli, F., Anzidei, M., Ferranti, L., Leoni, G., Scicchitano, G., Silenzi, S., 2011. Sea level change along the Italian coast during the Holocene and projections for the future. Quat. Int. 232 (1–2), 250–257.
LePera, E., Critelli, S., 1997. Sourceland controls on the composition of beach and fluvial sand of the northern Tyrrhenian coast of Calabria, Italy: implications for actualistic petrofacies. Sediment. Geol. 110 (1–2), 81–97.
LePera, E., Sorriso-Valvo, M., 2000. Weathering, erosion and sediment composition in a high-gradient river, Calabria, Italy. Earth Surf. Process. Landf. 25 (3), 277–292.
Liu, J.P., Xue, Z., Ross, K., Wang, H.J., Yang, Z.S., Li, A.C., Gao, S., 2009. Fate of Sediments Delivered to the Sea by Asian large Rivers. Sediment. Recor. 7 (4), 4–9.
Lobo, F.J., Ridente, D., 2014. Stratigraphic architecture and spatio-temporal variability of high-frequency (Milankovitch) depositional cycles on modern continental margins: an overview. Mar. Geol. 352, 215–247.
Lu, H., Fulthorpe, C.S., 2004. Controls on sequence stratigraphy of a middle Miocene–Holocene, current-swept, passive margin: offshore Canterbury Basin, New Zealand. Geol. Soc. Am. Bull. 116 (11–12), 1345–1366.
Manville, V., Németh, K., Kano, K., 2009. Source to sink: a review of three decades of progress in the understanding of volcaniclastic processes, deposits, and hazards. Sediment. Geol. 220 (3–4), 136–161.
Martorelli, E., Chiocci, F.L., Orlando, L., 2010. Imaging continental shelf shallow stratigraphy by using different high-resolution seismic sources: an example from the Calabro-Tyrrhenian margin (Mediterranean Sea). Braz. J. Oceanogr. 58, 55–66.
Meade, R.H., 1972. Transport and deposition of sediments in estuaries. Geol. Soc. America 133 (1), 91–120.
Meschis, M., Teza, G., Serpelloni, E., Elia, L., Lattanzi, G., di Donato, M., Castellaro, S., 2022. Refining rates of active Crustal Deformation in the Upper Plate of Subduction zones, Implied by Geological and Geodetic Data: the E-Dipping West Crati Fault, Southern Italy. Remote Sens. 14 (21), 5303.
Milliman, J.D., Syvitski, J.P., 1992. Geomorphic/tectonic control of sediment discharge to the ocean: the importance of small mountainous rivers. J. Geol. 100 (5), 525–544.
Millot, C., 1991. Mesoscale and seasonal variabilities of the circulation in the western Mediterranean. Dyn. Atmos. Oceans 15 (3–5), 179–214.
Montgomery, D.R., Foufoula-Georgiou, E., 1993. Channel network source representation using digital elevation models. Water Resour. Res. 29 (12), 3925–3934.
Muto, F., Robustelli, G., Scarciglia, F., Spina, V., Critelli, S., 2003. Geomorphology, tectonics and sedimentology of Late Quaternary fans between Guardia Piemontese and Paola (Tyrrhenian Coast of Calabria, Southern Italy). Il Quaternario—Italian J. Quatern. Sci. 16 (2), 217–229.
Nittrouer, C.A., 2003. Contrasting styles of off-shelf sediment accumulation in New Guinea. Mar. Geol. 196 (3–4), 105–125.
Olivetti, V., Cyr, A.J., Molin, P., Faccenna, C., Granger, D.E., 2012. Uplift history of the Sila Massif, southern Italy, deciphered from cosmogenic 10Be erosion rates and river longitudinal profile analysis. Tectonics 31 (3).
Ouimet, W.B., Whipple, K.X., Granger, D.E., 2009. Beyond threshold hillslopes: Channel adjustment to base-level fall in tectonically active mountain ranges. Geology 37 (7), 579–582.
Perry, C.T., Kench, P.S., O'Leary, M.J., Morgan, K.M., Januchowski-Hartley, F., 2015. Linking reef ecology to island building; parrotfish identified as major producers of island building sediment in the Maldives. Geology 43 (6), 503–506.
Pinardi, N., Masetti, E., 2000. Variability of the large scale general circulation of the Mediterranean Sea from observations and modelling: a review. Palaeogeogr. Palaeoclimatol. Palaeoecol. 158 (3–4), 153–173.
Pinardi, N., Korres, G., Lascaratos, A., Roussenov, V., Stanev, E., 1997. Numerical simulation of the interannual variability of the Mediterranean Sea upper ocean circulation. Geophys. Res. Lett. 24 (4), 425–428.
Pirrotta, C., Parrino, N., Pepe, F., Tansi, C., Monaco, C., 2022. Geomorphological and morphometric analyses of the Catanzaro trough (Central Calabrian Arc, Southern Italy): Seismotectonic implications. Geosciences 12 (9), 324.
Puig, P., Ogston, A.S., Mullenbach, B.L., Nittrouer, C.A., Sternberg, R.W., 2003. Shelf-to-canyon sediment-transport processes on the Eel continental margin (northern California). Mar. Geol. 193 (1–2), 129–149.
Puig, P., Durán, R., Muñoz, A., Elvira, E., Guillén, J., 2017. Submarine canyon-head morphologies and inferred sediment transport processes in the Alías-Almanzora canyon system (SW Mediterranean): on the role of the sediment supply. Mar. Geol. 393, 21–34.
Rabineau, M., Berné, S., Aslanian, D., Olivet, J.L., Joseph, P., Guillocheau, F., Bourillet, J. F., Le Drezen, E., Grangeon, D., 2005. Sedimentary sequences in the Gulf of Lion: a record of 100,000 years climatic cycles. Mar. Pet. Geol. 22 (6–7), 775–804.
Ridente, D., 2016. Releasing the sequence stratigraphy paradigm. Overview and perspectives. J. Geol. Soc. 173 (5), 845–853.
Ridente, D., Trincardi, F., 2005. Pleistocene "muddy" forced-regression deposits on the Adriatic shelf: a comparison with prodelta deposits of the late Holocene highstand mud wedge. Mar. Geol. 222–223, 213–233.
Robustelli, G., Muto, F., Scarciglia, F., Spina, V., Critelli, S., 2005. Eustatic and tectonic control on late Quaternary alluvial fans along the Tyrrhenian Sea coast of Calabria (South Italy). Quat. Sci. Rev. 24 (18–19), 2101–2119.
Roda-Boluda, D.C., D'Arcy, M., Whittaker, A.C., Gheorghiu, D.M., Rodés, Á., 2019. 10Be erosion rates controlled by transient response to normal faulting through incision and landsliding. Earth Planet. Sci. Lett. 507, 140–153.
Romagnoli, C., Casalbore, D., Chiocci, F.L., 2012. La Fossa Caldera breaching and submarine erosion (Vulcano island, Italy). Mar. Geol. 303, 87–98.
Ruello, M.R., Cinque, A., Di Donato, V., Molisso, F., Terrasi, F., Russo Ermolli, E., 2017. Interplay between sea level rise and tectonics in the Holocene evolution of the St. Eufemia Plain (Calabria, Italy). J. Coast. Conserv. 21, 903–915.
Sabato, L., Tropeano, M., 2004. Fiumara: a kind of high hazard river. Phys. Chemi. Earth, Parts 29 (10), 707–715.
Schwanghart, W., Scherler, D., 2014. Short Communication: TopoToolbox 2 – MATLAB-based software for topographic analysis and modeling in Earth surface sciences. Earth Surf. Dyn. 2 (1), 1–7.
Somme, T.O., Helland-Hansen, W., Martinsen, O.J., Thurmond, J.B., 2009. Relationships between morphological and sedimentological parameters in source-to-sink systems: a basis for predicting semi-quantitative characteristics in subsurface systems. Basin Res. 21, 361–387.
Sømme, T.O., Piper, D.J., Deptuck, M.E., Helland-Hansen, W., 2011. Linking onshore–offshore sediment dispersal in the Golo source-to-sink system (Corsica, France) during the late Quaternary. J. Sediment. Res. 81 (2), 118–137.
Sorriso-Valvo, M., Sylvester, A.G., 1993. The relationship between geology and landforms along a coastal mountain front, northern Calabria, Italy. Earth Surf. Process. Landf. 18, 257–273.

Stock, J., Dietrich, W.E., 2003. Valley incision by debris flows: evidence of a topographic signature. Water Resour. Res. 39 (4).
Trincardi, F., Correggiari, A., Roveri, M., 1994. Late Quaternary transgressive erosion and deposition in a modern epicontinental shelf: the Adriatic semienclosed basin. Geo-Mar. Lett. 14 (1), 41–51.
Trincardi, F., Correggiari, A., Field, M.E., Normark, W.R., 1995. Turbidite deposition from multiple sources; Quaternary Paola Basin (eastern Tyrrhenian Sea). J. Sediment. Res. 65 (4b), 469–483.
Tropeano, M., Cilumbriello, A., Sabato, L., Gallicchio, S., Grippa, A., Longhitano, S.G., Spilotro, G., 2013. Surface and subsurface of the Metaponto Coastal Plain (Gulf of Taranto—southern Italy): Present-day-vs LGM-landscape. Geomorphology 203, 115–131.
Vail, P.R., Hardenbol, J., Todd, R.G., 1984. Jurassic unconformities, chronostratigraphy, and sea-level changes from seismic stratigraphy and biostratigraphy. In: Schlee, J.S. (Ed.), Interregional Unconformities and Hydrocarbon Accumulation: American Association of Petroleum Geologists, Memoir, 36, pp. 129–144.
Van Wagoner, J.C., Posamentier, H.W., Mitchum, R.M., Vail, P.R., Sarg, J.F., Loutit, T.S., Hardenbol, J., 1988. An overview of the fundamentals of sequence stratigraphy and key definitions. In: Wilgus, et al. (Eds.), Sea-Level Changes: An Integrated Approach, 42. SEPM, Special Publication, pp. 39–45.
Van Wagoner, J.C., Mitchum, R.M., Campion, K.M., Rahmanian, V.D., 1990. Siliciclastic Sequence Stratigraphy in well Logs, Cores, and Outcrops: Concepts for High Resolution Correlation of Time and Facies. In: American Association of Petroleum Geologists, Methods in Exploration Series, 7, p. 55.
Walsh, J.P., Wiberg, P.L., Aalto, R., Nittrouer, C.A., Kuehl, S.A., 2016. Source-to-sink research: economy of the Earth's surface and its strata. Earth Sci. Rev. 153, 1–6.
Westaway, R., 1993. Quaternary uplift of southern Italy. J. Geophys. Res. Solid Earth 98 (B12), 21741–21772.
Whipple, K.X., Tucker, G.E., 1999. Dynamics of the stream-power river incision model: Implications for height limits of mountain ranges, landscape response timescales, and research needs. J. Geophys. Res. Solid Earth 104 (B8), 17661–17674.
Wobus, C., Whipple, K.X., Kirby, E., Snyder, N., Johnson, J., Spyropolou, K., et al., 2006. Tectonics from topography: Procedures, promise, and pitfalls. Spe. Paper Geol. Soc. America 398, 55–74.

Websites visited for downloading or visualizing data used for the manuscript

http://www.worldclim.org/bioclim.
https://asterweb.jpl.nasa.gov/gdem.asp.
https://www.copernicus.eu/en/copernicus-satellite-data-access.
https://www.isprambiente.gov.it/it/banche-dati/banche-dati-folder/suolo-e-territorio/dati-geognostici-e-geofisici.